

DSIA JOURNAL

A Quarterly Publication of the Defense Systems Information Analysis Center

Volume 6 • Number 3 • Summer 2019

A Multisensor System for Measuring the Light Output and Velocity of Live-Fired, Red Light-Emitting

PYROTECHNIC TRACERS

PAGE 26

PAGE 4

DISPOSAL OF INSENSITIVE MUNITIONS

PAGE 10

COMPUTATIONAL AND EXPERIMENTAL CHARACTERIZATION OF AN IMPROVISED, EXPLOSIVELY FORMED PENETRATOR

PAGE 17

INVESTIGATING FRICTION STIR WELDING IN ALUMINUM HULL STRUCTURES

PAGE 21

ADDITIVELY MANUFACTURED, SOLVENT-LOADED AP COMPOSITE PROPELLANT - PRINTER PARAMETER OPTIMIZATION



Distribution Statement A: Approved for public release; distribution is unlimited.



VOLUME 6 | NUMBER 3 | SUMMER 2019

Editor-in-Chief: Brian Benesch

Copy Editor: Maria Brady

Art Director: Melissa Gestido

On the Cover:

(Source: U.S Marine Corps)

The DSIAC Journal is a quarterly publication of the Defense Systems Information Analysis Center (DSIAC). DSIAC is a DoD Information Analysis Center (IAC) sponsored by the Defense Technical Information Center (DTIC) with policy oversight provided by the Office of the Under Secretary of Defense (OUSD) for Research and Engineering (R&E). DSIAC is operated by the SURVICE Engineering Company with support from Georgia Tech Research Institute, Texas Research Institute/Austin, and The Johns Hopkins University.

Copyright © 2019 by the SURVICE Engineering Company. This journal was developed by SURVICE under DSIAC contract FA8075-14-D-0001. The Government has unlimited free use of and access to this publication and its contents, in both print and electronic versions. Subject to the rights of the Government, this document (print and electronic versions) and the contents contained within it are protected by U.S. copyright law and may not be copied, automated, resold, or redistributed to multiple users without the written permission of DSIAC. If automation of the technical content for other than personal use, or for multiple simultaneous user access to the journal, is desired, please contact DSIAC at 443.360.4600 for written approval.

Distribution Statement A: Approved for public release; distribution is unlimited.

ISSN 2471-3392 (Print)
ISSN 2471-3406 (Online)



CONTENTS

- 4 Disposal of Insensitive Munitions ▶
EN Energetics
- 10 Computational and Experimental Characterization of an Improvised, Explosively Formed Penetrator ▶
WS Weapon Systems
- 17 Investigating Friction Stir Welding in Aluminum Hull Structures ▶
SV Survivability & Vulnerability
- 21 Additively Manufactured, Solvent-Loaded AP Composite Propellant – Printer Parameter Optimization ▶
AM Advanced Materials
- 26 A Multisensor System for Measuring the Light Output and Velocity of Live-Fired, Red Light-Emitting Pyrotechnic Tracers ▶
MS Military Sensing

CONTACT DSIAC

Ted Welsh
DSIAC Director

Brian Benesch
DSIAC Technical Project Lead

DSIAC HEADQUARTERS
4695 Millennium Drive
Belcamp, MD 21017-1505
Office: 443.360.4600
Fax: 410.272.6763
Email: contact@dsiac.org ▶

WPAFB SATELLITE OFFICE
704 TG/OL-AC/DSIAC
2700 D Street, Building 1661
Wright-Patterson AFB, OH 45433-7403
Office: 937.255.3828
DSN: 785.3828
Fax: 937.255.9673

DSIAC CONTRACTING OFFICER REPRESENTATIVE

Peggy M. Wagner (COR)
704 TG/OL-AC
2700 D Street, Building 1661
Wright-Patterson AFB, OH 45433-7403
Office: 937.255.6302

DSIAC PROGRAM MANAGEMENT ANALYST

Emese Horvath
IAC Program Management Office (DTIC-I)
8725 John J. Kingman Road
Fort Belvoir, VA 22060
Office: 571.448.9753

MESSAGE FROM THE EDITOR



By **Brian Benesch**

Ever notice all the magazines that line up near the register at a grocery store? You will never see the *DSIAC Journal* among them. That's because it is not an everyday magazine but, in fact, a journal. Although our journal is often mistakenly referred to as a magazine, it carries the distinction and traits of a scientific journal with a scientific audience.

The misconception in terminology might arise from similarities that our publication shares with typical magazines. We sport an aesthetically-pleasing, glossy cover, and our articles are interspersed with images, figures, and plots that illuminate the written content. In contrast, typical scholarly journals have plain covers and few-to-no images associated with their articles. Scholarly journal articles very rarely have any color and certainly do not have the eye-catching, lead-in imagery that we use on the first page of each one of our articles. For these reasons, casual readers of the *DSIAC Journal* may describe it as a magazine.

Nonetheless, we aim to incorporate important features in our publication that distinguish it as a journal. Most notably, our articles are written firsthand by researchers, scientists, or engineers to describe their own technical efforts, often in a very in-depth manner. Information in the articles is well referenced and typically contains a concluding section substantiated by the prior write-up. The articles are written so that they are intelligible to a technically proficient reader well versed in the defense systems community. Therefore, they are not necessarily intended to be accessible to the general public.

Further, our technical articles, while not peer reviewed in the same thorough way as scholarly journal articles, are reviewed by technical staff to verify the scientific merits of their content. Alternatively, magazine articles are written for the general public, often as second-hand accounts, and with content that is not fully sourced and referenced. Magazines are also frequently littered with advertisements, whereas our journal is ad free.

Concern of publication type (journal or magazine) involves more than just semantics. We strive to produce a journal-quality publication that authors and readers in our defense systems community can benefit from in sharing technical research, findings, and technology. We have set a certain expectation for our authors and readers. Authors should understand the level of publication they are contributing to before they submit their article and participate in our publication process. Readers should understand the type of content they expect to find in each *DSIAC Journal*.

We strive to produce a journal-quality publication that authors and readers in our defense systems community can benefit from in sharing technical research, findings, and technology.

What can you, as a reader, expect to find in the *DSIAC Journal*? We are committed to producing a quarterly journal that features technical articles exploring new ideas and emerging trends in defense systems science and engineering topics. Specifically, our chartered areas focus on advanced materials; autonomous systems; directed energy; energetics; military sensing; non-lethal weapons; reliability, maintainability, quality, supportability, and interoperability [RMQSI]; survivability & vulnerability; and weapon systems. Our articles will be technically substantive and yet accessible to the reader familiar with the defense systems community. Finally, the articles will be packaged together in a polished, visually appealing product published in print and digital formats.

Please enjoy this and all releases of our journal! ■

A handwritten signature in black ink that reads "Brian Benesch". The signature is fluid and cursive, with the first name "Brian" and last name "Benesch" clearly legible.

(Source: U.S. Marine Corps)



DISPOSAL OF INSENSITIVE MUNITIONS

By William Bagley

SUMMARY

This article addresses some of the challenges associated with explosive ordnance disposal (EOD) techniques when applied to insensitive munitions (IMs). The established

disposal techniques for conventional munitions or unexploded ordnance (UXO) typically involve high-order, sympathetic detonation caused by bare donor charges or applying specialized EOD shaped charges. Depending on design, shaped charges can induce either high- or low-order detonation when used with conventional munitions. These techniques have shown limitations when applied to IM. The gap between the

energy needed to achieve case penetration to enable access to explosive fill and the full initiation of the munition may be more difficult to achieve for insensitive high explosive (IHE)-filled UXO that have been exposed to violent stimuli, partially armed, armed, or partially functioned from failure to function as designed. The process of establishing new EOD methods for use against IM will require techniques used

to achieve high- and low-order reactions. This may be achieved by modifying techniques historically used for conventional munition disposal if developers can overcome the limitations of these techniques when applied to IM. This article discusses challenges associated with developing new IM EOD disposal methods and presents examples of existing and emerging technologies that may offer possible solutions.

BACKGROUND

In order to fulfill required missions, the U.S. Armed Services need to procure weapons with a high degree of effectiveness in sufficient volume for sustained combat operations while ensuring the greatest degree of safety as reasonably achievable to personnel and logistic assets. One way to support this goal is to design munitions that do not react violently to inadvertent stimuli. This approach presents an added benefit by complicating reuse by adversaries. As modern battlefields increasingly shift into populated urban centers, IM inventories represent a less-desirable target for terrorists and minimize the threat to surrounding communities. Insensitive munitions could potentially be more cost effective to transport if the goal of lower U.S. Department of Defense (DoD)/Department of Transportation hazard classification rankings can be achieved. In addition, the reduced probability of catastrophic accidents involving IM allows more munitions to be stored in a given area because of reduced, mandated quantity-distance separation requirements.

Developing appropriate procedures for disposal of explosive ordnance is mandated by Allied Explosive Ordnance Disposal Publication 10 and echoed in North Atlantic Treaty Organization

The established disposal techniques to conventional munitions or unexploded ordnance typically involve high-order, sympathetic detonation caused by bare donor charges or applying specialized EOD shaped charges.

(NATO) Standardization Agreement (STANAG) 2143 [1]. As a result of IM programs, many munitions that are increasingly less shock sensitive and have increased critical diameters are being fielded. This creates problems for EOD technicians while conducting a render-safe procedure and ordnance disposal procedures. Traditional EOD methods consist of a number of historically proven techniques—shock initiation by donor charge, directed energy attack (e.g., shaped charge), thermal initiation charge (thermite), and stand-off munitions disruptors. In addition, UXO disposal operations may require a nondetonating response when the situation will not allow high-order detonation disposal. As newer insensitive munitions are designed to prevent continuation of a violent reaction to external stimuli, achieving a complete or nearly complete low-order reaction presents its own unique set of challenges. Additionally, recent experience has highlighted the requirement to remove explosive ordnance from the operational theater to deny its reuse in improvised explosive

devices. This has led to significant dedication of resources in theater that utilize expedient methods of disposal.

In 2017, the Joint Service EOD Program Office completed an Analysis of Alternatives on IM disposal. While there is a commitment to remaining informed regarding what is being developed in the IM community, no specific path forward to addressing EOD needs for IM disposal was chosen at that time.

DISPOSAL PROCEDURES

Disposal of IM is an emerging issue in need of attention throughout the defense industry, governments, and humanitarian demining organizations. In 2012, the DoD used the Small Business Innovation Research program to solicit proposals for technology that can reliably cause detonating IM and/or bulk IHEs without large amounts of donor explosives [2]. Numerous DoD agencies, national labs, and defense contractors have, or are currently investing in, IM disposal technology development programs; however, little has been published in open forums. The NATO EOD Working Group has demonstrated interest but has not yet issued NATO guidance for IM disposal procedures.

Sympathetic Detonation

Sympathetic detonation is a disposal method that uses the influence of a donor explosive placed nearby to initiate a detonation in the target munition. Large IM-filled munitions present difficulties for disposal by open detonation due to the large amount of donor explosives required to initiate the munition and the risk of incomplete consumption of the explosive fill. Traditional methods of sympathetic detonation for conventional munitions by direct application of bare donor, high-explosive charges have failed to

reliably and repeatedly initiate and/or consume insensitive explosive fills during emergency destruction. Initial modifications of existing techniques required up to 400% more donor explosives and typically achieved only partial detonation. The increase in total explosive weight can exceed range limits previously set by conventional munition disposal allowances. Where munitions can be disposed by open detonation, incomplete destruction with large pieces of unreactive energetics typically results. This can create significant logistical hurdles, health, and safety concerns for explosive ordnance disposal personnel.

Countercharging IM-compliant, small-diameter munitions with large volumes of bulk conventional high explosives may lead to effective disposal. However, this can present a significant logistical burden and an unnecessary consumption of explosives. It may also increase the overall explosive hazard. These hazards are multiplied for disposal operation in high-threat environments. Experience from combat theater operations has demonstrated the requirement for economy of effort and the importance of limiting the risk to EOD operators.

Shaped Charge Attack

Manufactured shaped charge EOD tools capable of producing sufficient diameter jets have become an impractical proposition for dismounted EOD operations. A trend in recent years has been developing commercially-provided, user-filled shaped charge systems and, in some instances, offering a variety of liner materials and configurations. This approach has value in reducing the logistical burdens associated with prefilled, manufactured EOD charge systems. Reliability and repeatability of the explosive effect from the tool and target munition response will dictate

acceptance from the EOD community. Shaped charge attacks also have potential use for low-cost, planned demilitarization of IM.

Commercial Shaped Charges

Commercial products include various-sized, shaped charges, some with specific application such as underwater demolitions. Both manufactured, flexible, linear shaped charges and hand-packed, high-explosive shaped charges have yielded predictable results when applied to IM regarding warhead case rupturing and segmenting rocket motors.

Thunder Range (organization 6647) of Sandia National Laboratories, NM, recently demonstrated the Cylindrical Dynamic Access Tool (CDAT) to be an effective means of disposal of certain IHE munitions using 1 lb of hand-packed explosives (see Figure 1). This technique can be improvised by the user, or the plastic body may be purchased through a commercial vendor (Team Technologies, Albuquerque, NM). The CDAT's production plastic body is a user-configurable, multiuse charge with advanced capabilities, including a



Figure 1: Placement of Cylindrical Dynamic Access Tool Prior to Initiation (Source: Sandia National Laboratories).

shaped charge, an explosively formed penetrator, and a contact charge. Energetic materials required to fill it are PETN-based sheet explosive and plasticized, moldable explosives like C-4 or Syntex.

The Alford Technologies' Krakatoa is a 100- x 100-mm charge container body with two load position options to accommodate either 500 or 1000 g of plastic explosive (see Figure 2). The main body of the larger Vesuvius charge is approximately 160 mm long, 160 mm in diameter, and capable of holding ~4 kg of plastic explosives. The size and performance characteristics of the Vesuvius make it a suitable surrogate for testing armor against improvised, explosively-formed penetrators. No

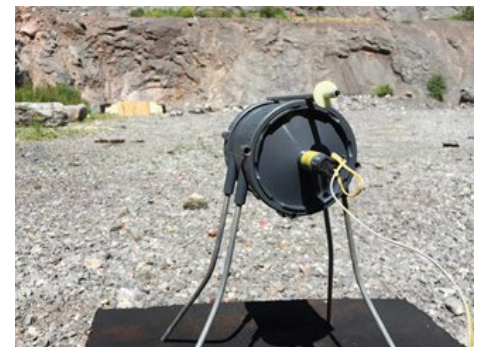


Figure 2: Alford Technologies' Krakatoa disruptor (Source: Alford Technologies).

open-source test data are available assessing these commercially-available tools' performance against IM targets [3].

Northrop Grumman (formerly, ATK Ordnance and Ground Systems) produces the SM-EOD family of explosive charges consisting of RDX, wax, and graphite, initiated with a No. 8 or equivalent blasting cap. The SM-EODs are manufactured in accordance with MIL and NATO standards and available in six calibers.

Shaped Charge Jet Attack

The response of a munition attack by a shaped charge jet depends on many factors, including characteristics of the fill, confinement, case thickness, and jet tip velocity and diameter. If a jet is sufficiently fast, its penetration velocity will exceed the explosive's detonation velocity and the technique may achieve a steady-state detonation. Lower-velocity jet results in slower penetration, where the detonation wave precedes the penetration process to consume the explosive. Achieving sufficient penetration to ensure complete consumption of insensitive fills without initiating a high-order detonation requires complex geometry specifically tailored to the target munition.

It is possible to determine the approximate charge diameter necessary to reliably initiate insensitive explosives through a shaped charge jet attack given the jet tip velocity, critical diameter of the explosive fill, and case composition and thickness. Held calculated a minimal threshold value for initiating explosives to be a product of the jet tip's velocity squared multiplied by the jet tip's diameter [4].

$$H = V^2d. \tag{1}$$

Patel and Voisin have shown that Held's criteria values correlate to critical diameters [5, 6]:

$$Held\ criterion = 1.278 (C_d (mm))^{1.73726}. \tag{2}$$

Pope and Baker calculated the diameter of the jet tip to be approximately 0.04133 x the diameter of the shaped charge [7]:

$$d_{jet} = 0.04133 d_{warhead}. \tag{3}$$

By using the known jet tip velocity and compensating for decreased velocity due to case penetration, a rough estimate can be determined for the size of the shaped charge needed to initiate a given munition. For example, Pope and Baker calculated a minimal shaped charge diameter for an IMX-101 charge at critical diameter [7]. Their results are summarized in Table 1.

Majerus reported developing advanced shaped charges with roughly doubled jet diameters than those produced by conventional shaped charge designs of the same size [9]. Currently, the shaped charge liners produce large-diameter sections at lower jet velocities. However, modifying the shaped charge design to achieve the necessary jet tip velocity at increased jet tip diameter is possible. An advanced shaped charge design that produces roughly doubled jet diameters could potentially halve the required shaped charge disruptor diameters.

Shock Loading

The response of energetic materials to low-amplitude/long-duration impact and shock loading may have potential application for disposal of IM. It is possible that an initial shock-loading event (e.g., impact flyer plate) could sensitize an insensitive fill to subsequent impacts, which may then lead to a more violent reaction than would have occurred in response to a single flyer plate impact. Experiments by Haskins et al. demonstrated that detonation via an unknown detonation transition or deflagration-to-detonation transition process may be produced through intentionally applying multiple fragment impacts [10]. A related phenomena using colliding shock waves generated by two simultaneously-initiated bare donor charges is under investigation as a possible technique for IM disposal.

Explosively-Generated Plasma (EGP)

EGP is created by focusing explosive ejecta through a conical waveguide (e.g., Imhoff cones) that compresses the gasses to the extent where plasma is produced. Plasma can travel at velocities as high as 21,000 km/s, while producing temperatures as high as 20,000 K [8]. The Naval Surface Warfare Center Indian Head Explosive Ordnance Disposal Technology Division demonstrated that plasma can penetrate ordnance casing without

Table 1: Held's Criterion Used to Predict Shaped Charge Diameters [8]

HELD VALUE V ² d	JET VELOCITY (mm/μs)	JET DIAMETER (mm)	SHAPED CHARGE DIAMETER (mm)
1853.6	10	18.54	448
1853.6	8	28.96	700

fragmentation or deformation through the plasma ablation process. When plasma interacts with the munition case, the energy is transformed into heat, leading to melting and evaporating the case material at the interaction point. After penetration, the EGP causes a high-temperature chemical decomposition, resulting in deflagration of conventional energetic fills.

MUNITION MARKING

Positive identification of all UXO is required prior to performing a render-safe procedure or disposal operations. Recently ratified changes to Allied Ordnance Publication (AOP) 2, the NATO standard that governs marking munitions, include the requirement for marking the explosive name or official designation by stenciled or permanent marking every 90 degrees around the body [11]. This is mandatory for all newly-manufactured munitions from 20-mm and larger-caliber munitions, including aircraft bombs. The U.S. Joint Ordnance Technical Publication (JOTP) 70 amends this NATO requirement to only identify munitions with less-sensitive explosive fills [12].

Additionally, JOTP-70 provides alternate marking options if the markings negatively impact IM mitigation measures such as the thermal protective coating. In these instances, the marking may be applied to a less-vulnerable part of the munition, typically engraved in the baseplate. These updates will assist EOD technicians in distinguishing IM from their more sensitive counterparts and apply appropriate tools and techniques for disposal operations. Preliminary research efforts have studied using radio frequency ID tags for artillery rounds so that EOD teams can unambiguously identify UXO.

HEALTH CONSIDERATIONS

Part of the development of any new weapon system is considering toxicology of new formulations and its life-cycle impact from raw materials, manufacture, use, and disposal. Initial estimates for potential health impacts to EOD personnel were derived from exposure rates established through studies of conventional munitions disposal. Field testing munitions for energetics residue deposition demonstrated that a significant portion of some energetic compounds remained after detonation. Also concerning is that conventional disposal techniques applied to next generation IM often fail, resulting in releasing wholly-unreacted or partially-reacted fills and potentially increasing exposure and resulting health complications.

A significant amount of work has been dedicated to measuring the amount

of explosives remaining on the ground following the high-order detonation of conventional explosives. In May 2012, Strategic Environmental Research and Development Program (SERDP) investigated the life-cycle environmental impacts of the first generation of IM and issued an information paper that recommended reclassifying first-generation IM munitions to Condition Code B: Restricted from Training Use for all DoD assets [13]. Training facilities that used the rounds were notified through a DoD directive, and demilitarization facilities were alerted to the issue. Mortar rounds containing the IHE PAX-21 were tested in March 2012, and surface residue samples were collected following high-order, single-round, blow-in-place detonations. The results of the work are summarized in Table 2. Although the organic component of the IHE functioned properly, high amounts of perchlorate and other constituent residue rates were found.

Table 2: Results of the Deposition Rates and Detonation Efficiency for the EOD Scenarios of an IM Round [14]

SCENARIO	NUMBER OF REPLICATES	DNAN DEPOSITION RATE (%)	NTO DEPOSITION RATE (%)	DETONATION EFFICIENCY (%)
1: Full-order detonation	5	0.001	0.002	99.999
2: 5 blocks of C-4 around the charge	5	6	26	83.7
3: 2 blocks of C-4, one on each side	4	13	43	72.1
4: 2 blocks of C-4, at the nose, optimized configuration	3	6	0.3	97.4
5: 67-mm shaped charge on the side	3	1	10	93.9
6: 33-mm shaped charge aimed at the nose	2	0.6	1	99.1
7: 67-mm shaped charge aimed at the nose	2	53	74	40.5
8: 67-mm shaped charge aimed at the back	2	29	26	74.3
9: 84-mm shaped charge aimed at the back	1	0.04	0	99.8
	3	0.001	0.0001	99.999

TOXICITY

The U.S. Army Public Health Center (USAPHC) developed a phased process to assess environmental, safety, and occupational health consequences of existing and emerging energetic material. This program assesses potential impacts to human health and environmental effects arising from exposure to energetic material, precursors, and residual contamination in soil, surface water, and ground water. Though planned demilitarization is addressed in the scope of USAPHC's mission, emergency response performed by EOD is not.

Results for nitroguanidine (NQ), though not an IHE, are included in Table 3 for comparison. Two components found in insensitive munition formulations have limited human toxicity data, 3-nitro-1,2,4-triazol-5-one (NTO), and 2,4-dinitroanisole (DNAN), but studies involving rats and monkeys have recently been completed. The studies found that the primary adverse effect from subchronic oral NTO exposure was hypospermia, and the effects from DNAN exposure include reduced body weight, anemia, and neurotoxicity [15]. USAPHC reporting suggests that human toxicity effects from DNAN exposure are expected to be similar to most other energetic compounds and slightly less than TNT. High daily exposure to NTO affects sperm production. No chronic data are available for DNAN or NTO.

CONCLUSIONS

Munitions with newer, less-sensitive explosive compositions in the main charge present challenges for open-detonation disposal by using conventional EOD techniques. The lack of reliability of bare donor charge disposal techniques to consume nearly all insensitive munition fills

Table 3: Relative Toxicity of IMX-101 and Constituents [15]

CONSTITUENT	ACUTE ORAL ^a [mgkg ⁻¹]	14-DAY ORAL ^b [mgkg ⁻¹ -d]	90-DAY ORAL ^c [mgkg ⁻¹ -d]	OTHER ^d [mgkg ⁻¹ -d]
NQ	>5000	NA	NA	—
DNAN	199	11.4	2.3	—
NTO	>5000	167	40	120
IMX-101	1100	31c	—	—

^a Median lethal dose in rats.

^b BMDL10.

^c Based on changes in splenic mass.

^d Reproductive/developmental studies.

necessitates adopting improved disposal techniques. Shaped charge attack (particularly, shaped charge jet attack) is a mature technology that represents a potential solution and is already well understood and accepted within the EOD community. Proliferating advanced shaped charge warhead design represents a threat to global security; export restrictions will likely limit availability to nonmilitary UXO disposal technicians.

Equally important, health and environmental impacts of exposure to IHE detonation products and unreacted material have not been fully explored. Continued research into potential health effects of fielded munitions and emerging insensitive energetic compounds is necessary to ensure the safety of personnel throughout the full life cycle of IM development, manufacture, use, and disposal. ■

REFERENCES

- [1] NATO STANAG 2143/AEODP-10 EOD. "Principles and Minimum Standards of Proficiency," 2014.
- [2] SBIR STTR. "Insensitive Munitions Disposal Attack." <https://www.sbir.gov/node/372782>, accessed May 2018.
- [3] Alford Technologies. <https://explosives.net/>, accessed July 2018.
- [4] Held, M. "Initierung von Sprengstoffen, ein Vielschichtiges Problem der Detonationsphysik." *Explosivstoff*, (translated by Lawrence Livermore National Laboratory as Ref. 02973, 1980), vol. 5, pp. 2-17, 1968.
- [5] Patel, R. "Investigation of Possible Correlations Between Burney Constant, Held Criteria, and Critical Diameter." ARAET-TR-06022, U.S. Army Armament Research,

Development and Engineering Center, Picatinny Arsenal, NJ, January 2007.

[6] Voisin, M. "Critical Diameter Correlations." MSIAC Report L-202, September 2016.

[7] Pope, M., and E. Baker. "Insensitive Munitions Explosive Ordnance Disposal Challenges." The 2018 Insensitive Munitions & Energetic Materials Technology Symposium, Portland, OR, 2018.

[8] Tasker, D., V. Whitley, and C. Johnson. "The Interaction of Explosively Generated Plasma With Explosives." American Institute of Physics Conference Proceedings, 2017.

[9] Majerus, M., and R. Brown. "Incorporation of Constant Velocity Elements in a Shaped Charge Jet for Special Applications." The 17th International Symposium on Detonation, vol. 2, p. 185, 1998.

[10] Haskins, P. J., R. I. Briggs, D. W. Leeming, N. White, and P. Cheese. "Dual Fragment Impact of PBX Charges." APS Topical Conference on the Shock Compression of Matter, 2017.

[11] NATO-AOP-2. "Identification of Ammunition," 2017.

[12] JOTP-070. "Identification Marking for Munitions." Joint Services Munition Safety Test Working Group, 2013.

[13] Walsh, M., S. Thiboutot, and B. Gullett. "Characterization of Residues From the Detonation of Insensitive Munitions: SERDP Project ER-2219," 2017.

[14] Brousseau, P., S. Thiboutot, and E. Diaz. "Explosives Ordnance Disposal (EOD) of Insensitive Munitions: Challenges and Solutions." Defence R&D Canada - Valcartier Research Center, 2018.

[15] Johnson, M., W. Eck, and E. Lent. "Toxicity of Insensitive Munition (IMX) Formulations and Components." *Propellants Explosives and Pyrotechnics*, vol. 42, pp. 9-16, 2017.

BIOGRAPHY

WILLIAM BAGLEY is an associate research engineer supporting energetics research and humanitarian demining programs at the Johns Hopkins University Whiting School of Engineering's Energetics Research Group. He also serves as the principal technical representative to the Joint Army Navy NASA Air Force (JANNAF) Interagency Propulsion Committee's Safety and Environmental Protection Subcommittee, the Propellant and Explosives Development and Characterization Subcommittee, and the Propulsion Systems Hazards Subcommittee and co-chairs the JANNAF Homemade Explosives Mission Area. He is a member of the International Association of Bomb Technicians and Investigators, the National Defense Industrial Association, and a Senior Explosive Ordnance Disposal Technician. Mr. Bagley is a graduate of the University of Maine and the Navy School of Explosive Ordnance Disposal.

Computational
and Experimental
Characterization of an

IMPROVISED, EXPLOSIVELY FORMED PENETRATOR

By Stanley DeFisher and Greg
Stunzenas

INTRODUCTION

Improvised explosive devices (IEDs) have proven to be highly lethal tools frequently used in asymmetric warfare. This has been particularly true of explosively formed penetrator (EFP)-based IEDs. Many of these devices are either manufactured

by foreign entities, in the manner in which “ordinary” production EFPs are produced, or they are crudely manufactured in a local setting. Regardless of the precise nature and location of their manufacture, however, they are often produced so imprecisely that proper formation of the EFP appears to have been an afterthought relative to simply inflicting damage against thinned vehicles and their occupants. The Combat Capabilities Development Command Armaments

Center (CCDC AC) characterized the performance of a simple, improvised device found in a foreign theater. This article outlines the effort to characterize the penetration performance of three improvised, copper, 4-inch-diameter EFPs recovered from the field. High-rate continuum modeling was used to understand the limits of the penetration capability of these devices and the implications of the manner in which they were produced so that the threat they pose could be accurately assessed.



In the most recent campaigns conducted by the United States and its allies, EFPs have been used against friendly forces with a high degree of effectiveness [1–3]. Later in the war as standard military-grade devices became too difficult or dangerous to obtain, homemade explosives started entering the scene. Not only did the types of explosives used to drive IEDs change, but their nature changed as well. In Iraq, there was a rapid change from the initial use of buried military-grade ordnance to improvised explosively formed penetrators (EFPs). In 2004, EFPs made their initial entrance into the Iraqi theater [4–7]. Because of a variety of tactical benefits, EFPs were often chosen by insurgents against coalition vehicles.

The lethal effectiveness of EFP IEDs motivated a rapid and extensive change in coalition tactics, techniques, and procedures, including the use of electronic and physical countermeasures like Warlock and Rhino, among others [8–10]. In as early as 2003, high-mobility, multi-wheeled vehicle (HMMWV) armor levels increased. Later in 2007, mine-resistant, ambush-protected vehicles like the Cougars and Buffalo began to see initial operational use [11, 12]. As a result of dwindling stockpiles of military-grade munitions and explosives, insurgents resorted to using improvised EFPs. The liner shown in Figure 1 is an improvised, 4-inch-diameter, copper EFP. The ultimate goal of this effort was to understand and characterize the performance of this device.

CHARACTERIZATION MODELING

In order to characterize the potential performance of this EFP, a computer model first had to be developed from previously-acquired samples. One of these liners can be seen in Figure 1.

From visual examination of this liner, it appears to have been pressed from low-purity copper, measuring roughly 3 mm thick. The liner depth measured 0.85 inches, a value that is only approximately 22% of the total liner diameter and is indicative of a lack of familiarity with traditional EFP designs. By our standards, this liner was crudely formed—composed of at least two different radii joined by a discontinuity. Subsequently, its performance was anticipated to be low because prior experimental observation of devices like these showed that the penetrator tended to break up only a short distance away from its original positions [13].



Figure 1: Improved Liner (Source: CCDC AC).

It appears as if minimal machining was conducted to clean up the outer circumference. An immediately apparent artifact of its manufacturing technique (observable in Figure 1) was the existence of a flat on both surfaces. This flat resulted in a noticeable discontinuity where it met the radii on both sides of the liner surface.

Although no body was recovered, it was assumed that the device was designed to be assembled inside a plastic housing. The length-to-diameter ratio of this body was kept to 1 for convenience. Composition C-4 was used as the driving explosive because of its availability and ease of use. From prior experience, a device of this caliber and precision was believed to be accurate out to maximum range of approximately 50 ft, with a “modest” penetration potential of only about 1.5 inches of steel. This was more than enough to penetrate thin-skinned vehicles.

Before proceeding with experimental characterization, CCDC engineers created a baseline solid model using PTC Creo from somewhat crude measurements taken using a Vernier caliper (Figure 2).

To generate this model, the following simplifying assumptions had to be made: the liner had a constant thickness of 3 mm, and the curvature of the liner was composed of two different curves that met at the surface

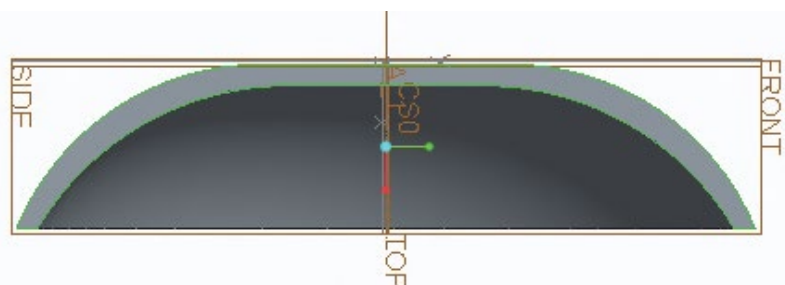


Figure 2: Improved EFP Solid Model (Source: CCDC AC).

discontinuity previously discussed. Although little was known about how this device was loaded, with what explosive, and whether or not it was boosted among other variables, a simplified set of simulations was generated.

All simulations were conducted using Lawrence Livermore National Laboratories code ALE3D (Table 1). An example of the baseline simulation at time 0 can be seen in Figure 3. An early time snapshot shows it folding rearward and breaking in Figure 4. A Johnson-Cook constitutive model was used for the copper liner in all simulations. The body was modeled using a Mie-Grüneisen equation of state, and the target was modeled using an internal material model. Approximately 10 elements per centimeter were used for all simulations.

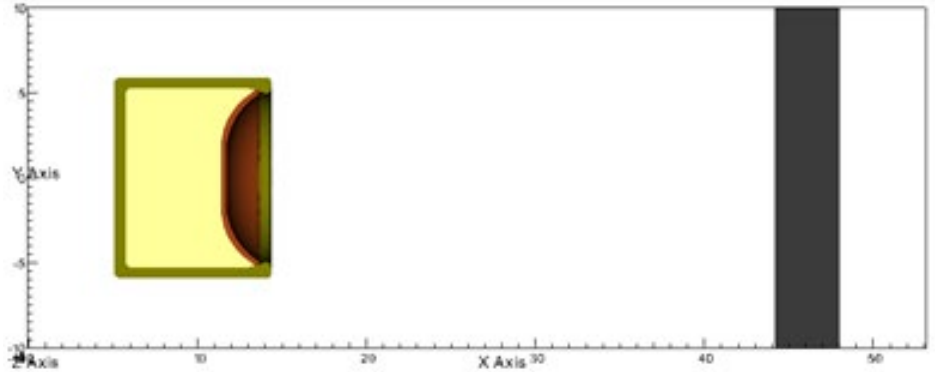


Figure 3: Baseline Penetration Model (Source: CCDC AC).

Table 1: Baseline Simulations

SIMULATION	TARGET	TARGET THICKNESS (inches)
1	No	NA
2	Yes	1.5
3	No	NA
4	Yes	1.5
5	No	NA
6	Yes	1.5

After only about 60 μ s, the penetrator tip separated from the rest of the body. This was not surprising given the visible discontinuity in the liner. Predictably, the velocity of the broken tip was much higher at around 2.2 km/s, while the remaining penetrator travelled at only around 1.5 km/s. Because the penetrator was both hollow and broken, it was highly likely that the penetration performance would be low. The computational results are tabulated in Table 2.

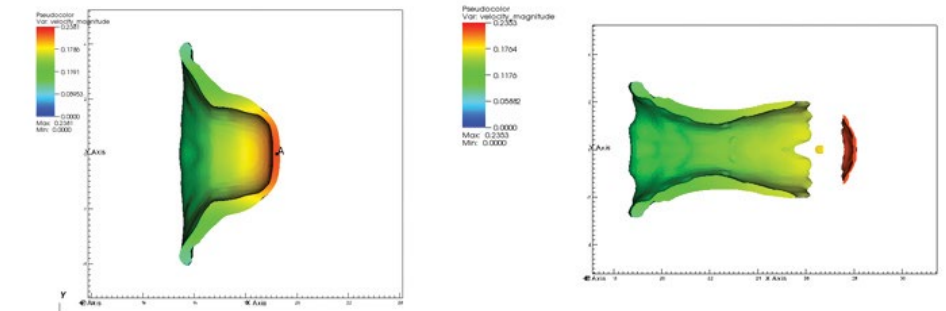


Figure 4: Baseline Model at 50 and 90 μ s (Source: CCDC AC).

Table 2: Baseline Performance

SIMULATION	LINER	COMPLETE PERFORATION
2	Baseline	No
4	Baseline	No
6	Baseline	No

LINER MEASUREMENT AND TESTING

Subsequent to initial modeling, a coordinate measuring machine (CMM) was used to verify the degree of agreement with the previous baseline and understand liner consistency and symmetry. It is important to point out that because these liners were not created from a solid model,

no solid modeling profile data were obtainable and, therefore, the data normally used for comparison did not exist. Perpendicular diameters were measured on both surfaces and broken down into two parts regarding their coordinate system. They were labeled as Zplus, Zminus, Xplus, and Xminus lines, with the positive y direction normal to the air side of the liner. Two circumferential measurements were also taken at different radii to assess profile consistency. An outline of a simplified set of this data can be seen in Figure 5.

All of the radial measurement data were then plotted to highlight any asymmetries, as shown in Figure 6. Although each liner had an average diameter measuring a little over 4 inches, CMM data were generally

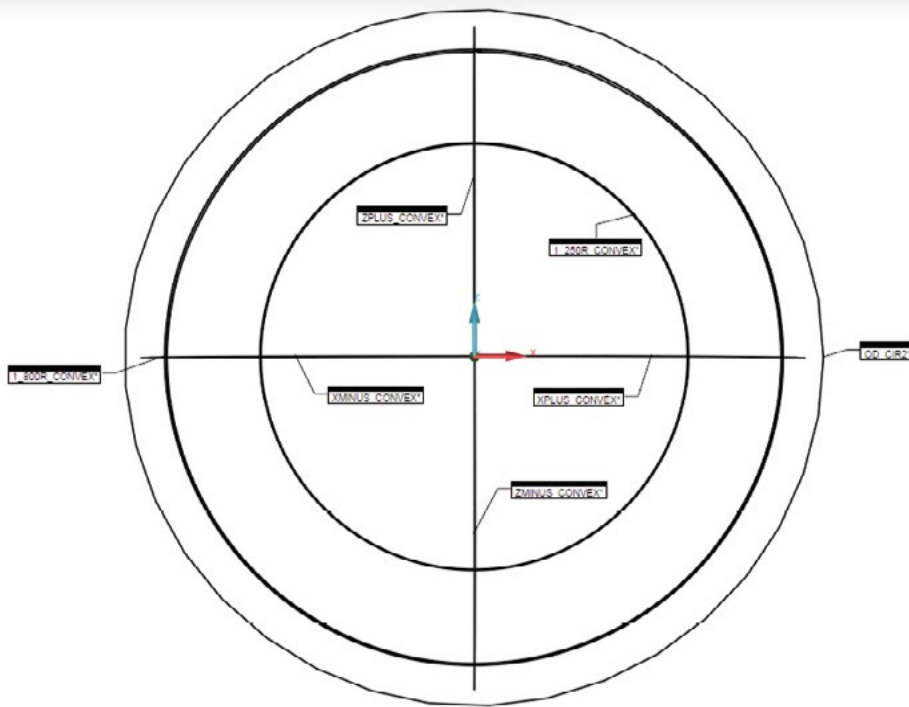


Figure 5: CMM Profile Measurements (Source: CCDC AC).

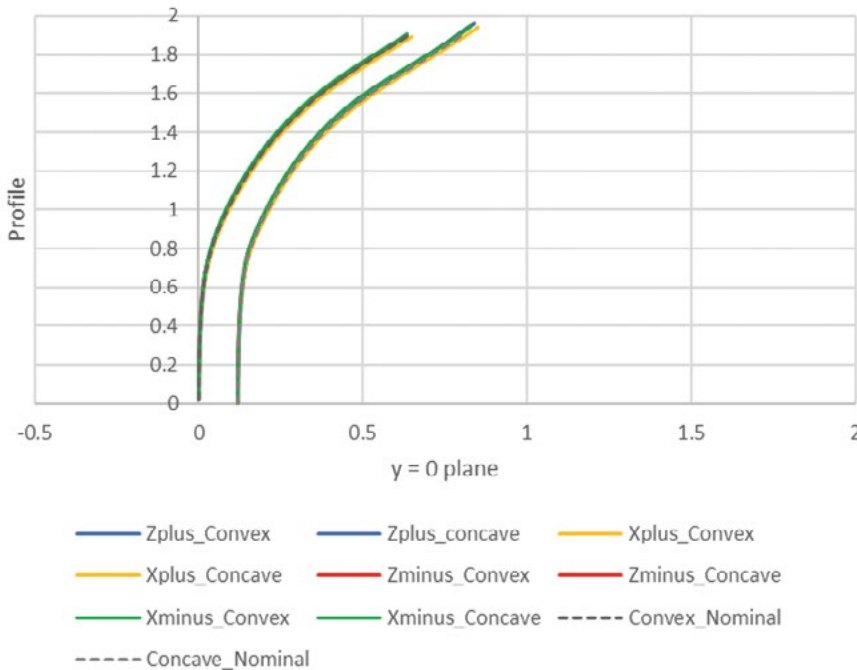


Figure 6: Liner 1 Profile Measurements (Source: CCDC AC).

Whatever manufacturing technique was used, it resulted in reasonably consistent results near the liner’s apex, with a far greater degree of variability near the outermost diameter. Tabulated measurement results are listed in Table 3.

These values were calculated by subtracting all of the values taken in the y direction on the concave side of the liner from those on the convex side. They were not measured normal to either the convex or concave surface but were simply differences in the measured y values taken along the various radial lines at different y points. If we disregard this somewhat crude numerical technique, we note several important features. For example, even though each line seems to indicate that liner measurement varies less than 0.0005 inches at the apex, there is a consistent but slight thinning of the material as one proceeds outward along the radial direction. What results is a variable liner profile that is thickest at the apex and outer diameter, with a thinner portion between the two. This was almost certainly an artifact of the manufacturing technique.

Secondly, it is apparent that these liners were not perfectly symmetric. From one quadrant to the next, maximum thicknesses were measured at different axial locations. In the second quadrant, a maximum liner thickness was measured at over 0.5 inches from the origin of the axis; however, this value was closer to 0.9 inches in the first quadrant. This is a tremendous difference that can only contribute to degraded performance. When these variations are coupled with others in high-explosive type, density, and metallurgical quality, penetration and accuracy are likely to suffer appreciably. We were unable to test accuracy over distance, however, because of the short range of our test facility.

only recorded out to a little under that diameter, as the process used to part the liner near the outer diameter left a rough, beveled outer edge. As a

result, including any data past the outer circumference would have appeared to decrease the liner’s geometric fidelity, so it was disregarded.

Table 3: Part 1 Liner Thickness Variations

LINE	APEX THICKNESS (Inches)	MIN THICKNESS (Inches)	MAX THICKNESS (Inches)	Y LOCATION (min/max inches)
Zplus	0.118	0.114	0.166	0.146/0.690
Xplus	0.118	0.114	0.170	0.144/outer diameter
Zminus	0.118	0.114	0.170	0.142/outer diameter
Xminus	0.118	0.114	0.171	0.143/0.709

When these variations are coupled with others in high-explosive type, density, and metallurgical quality, penetration and accuracy are likely to suffer appreciably.

Further variations can be seen by examining the data measured at the two radial distances shown in Figure 5. When we look at the data along these circles and compare them to ideal circles of identical radii, we see that the liner thickness varies from over 0.001 inches to almost 0.005 inches. This too is an appreciable difference that would not ordinarily be acceptable in an environment necessary to produce high-performance liners.

The CMM data we collected were limited because of the speed with which the results of this evaluation were required. Even if more data had been gathered, it would have been prohibitively difficult to use this information to generate a higher-fidelity, solid model. With the tools we had at the time, we would have had to make assumptions about how the liner transitioned from one quadrant to the next. If we only measured two

radial lines along a single diameter, we might assume that if the thicknesses were different, it changed linearly from one quadrant to the next. This would have been without any physical basis but would have made the problem numerically more tractable. As a result, the modeling used at least a subset of the four-point quadrant data shown in Figure 6 as this was an approximation that allowed a reasonable degree of error while minimizing other errors.

The first test we conducted used 150-kV x-ray heads fired at 190 and 350 μ s of delay from initiation time. The components' mass is tabulated in Table 4. Late times were chosen to accommodate the test configuration and the need to protect the x-ray films. We could not obtain early formation times prior to 130 μ s, making any comparison to the early time formation predicted via modeling impossible. The test setup is shown in Figure 7, while the model and x-rays can be seen in Figure 8.

Table 4: Shots 1 and 2 Mass

PART	LINER	EXPLOSIVE	BODY
Mass (g)	263.6	1029.8	248.8
	264.5	1077.2	249.5

Unfortunately, the segment of shot 1 film containing the fiducial rod was damaged. As a result, measuring velocity had to be conducted differently from the manner in which it would ordinarily be obtained. Instead, the distance

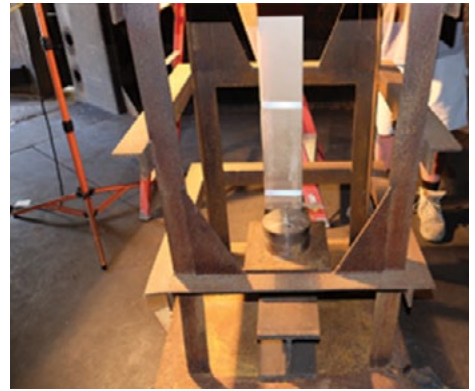
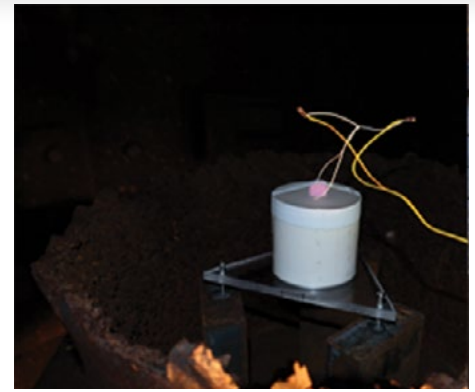


Figure 7: Test Setup (Source: CCDC AC).

the particles traveled was measured from the film. This distance, combined with knowing the times at which x-rays were fired, provided a somewhat crude mechanism to measure tip velocity (of the broken region) for shot 1 of 2.4 km/s. The calculated velocity was 2.3 km/s. The first large "particle" velocities measured roughly 1.9 and 1.85 km/s for shots 1 and 2, respectively. For shot 2, the lead particle had already exited the film area, so no calculation of velocity was possible. Penetration for both shots was in line with the higher end of the predicted value of 1.5 to 1.75 inches. Both target plates exhibited peripheral damage indicative of the fragmentation shown on the x-ray films (Figure 9).

Experiments and modeling resulted in general agreement for predicted velocity and penetration depth, with appreciable differences with the breakup. The copper was modeled using the well-

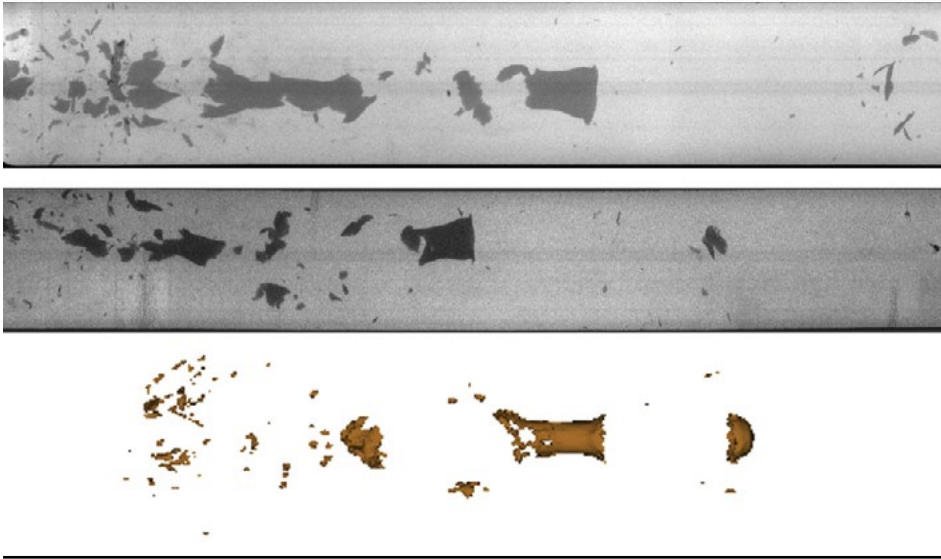


Figure 8: Late Time X-rays Taken at 190 and 350 μ s (Top and Middle) Compared to the Model at 350 μ s (Bottom) (Source: CCDC AC).



Figure 9: Steel witness plate penetration for Shot 1 (Left) and Shot 2 (Right) (Source: CCDC AC).

known Johnson-Cook constitutive equation with failure. (This type of model is usually applied to high-quality, high-purity copper.) The pedigree of the tested liner was completely unknown but believed to be a common, industrially-obtainable grade. Based on the x-rays taken during flight, the liner failed in a manner that could only be described as brittle. Whether the copper comes from sheet or bar stock, is forged from ingot, or is pure makes a tremendous difference in performance. In our estimation, these liners were unlikely to have come from high-quality copper used in traditional designs for which the Johnson-Cook model is most typically applied.

The initial metallurgical condition was also unknown, as was the heat treatment and level of work that were put into the material. Judging by the precision of the liner, however, it was highly likely that no additional heat treatment occurred. As a result, the ductility of the tested liner was likely far lower than modeled. Relative to other x-rayed EFPs, it appears as if the failure exhibited by this liner was brittle in nature. We believe that the type of copper used in these liners was electrolytic tough pitch (ETP). This type of copper is not commonly used in modern, high-performance EFPs because of its deleterious effect on performance.

Although there were numerous and appreciable imperfections in this liner, it is highly probable that its performance against thin-skinned vehicles like trucks or HMMWVs would be sufficient.

CONCLUSIONS

The baseline performance of an improvised, copper EFP was modeled using ALE3D. Agreement between the prediction and experimental data varied, with only modest agreement for early time formation. Predicted penetration performance agreed much better with modeling. Although there are likely a number of causes for early time formation differences, our primary hypothesis is that the material model we used to model the copper was different from the actual copper used in the item.

In the absence of compositional analysis, attributable to only having a low number of test articles, and because the constitutive and failure models depend upon such a composition, it is impossible to determine if this was the precise cause of the differences. There were, however, several other potential reasons for the observed variation between modeling and experiment. These include, but are not limited to, the simplified liner symmetry and profile necessary to begin modeling. From testing, we can safely conclude that although there were numerous and appreciable imperfections in this liner, it

is highly probable that its performance against thin-skinned vehicles like trucks or HMMWVs would be sufficient, albeit inconsistent, depending on the quality of the explosive loading, type of housing, and precision of assembly, among other factors. ■

REFERENCES

- [1] Welch, A. "Iraq – The Evolution of the IED." CBRNE World, http://www.cbrneworld.com/_uploads/download_magazines/08_autumn_IRAQ_EVOLUTION_OF_THE_IED.pdf, 2008.
- [2] Fahim, K., and L. Sly. "Lethal Roadside Bomb That Killed Scores of U.S. Troops Reappears in Iraq." *The Washington Post*, October 2017.
- [3] Eisenstadt, M., M. Knights, and A. Ali. "Iran's Influence in Iraq Countering Tehran's Whole-of-Government Approach." Policy focus #111, <https://www.washingtoninstitute.org/uploads/Documents/pubs/PolicyFocus111.pdf>, April 2011.
- [4] Conroy, S. "U.S. Sees New Weapon in Iraq: Iranian EFPs." CBS News, <https://www.washingtoninstitute.org/uploads/Documents/pubs/PolicyFocus111.pdf>, 11 February 2007.
- [5] Hambling, D. "EFP In Iraq: Deadly Numbers." <https://www.wired.com/2007/08/superbombs-the/>, 22 August 2007.
- [6] Crown. "The Report of the Iraq Inquiry. Report of a Committee of Privy Counsellors." United Kingdom House of Commons report, vol. XI, <http://www.gov.uk/government/publications>, 2016.
- [7] Morgan, D. "Iraq Sunni Insurgents Turn to Armor-Piercing Bombs." Reuters, 7 February 2008.
- [8] Russ, D. "The Silent War." <https://civilianmilitary-intelligencegroup.com/8264/the-silent-war-bombers-versus-jammers>, 10 July 2011.
- [9] Joint Improvised Explosive Device Defeat Organization (JIEDO). "Attack the Network – Defeat the Device – Train the Force." Annual report, 2008.
- [10] JIEDO. "DOD's Fight Against IEDs Today and Tomorrow." U.S. House of Representatives Committee on Armed Services Subcommittee on Oversight and Investigations, November 2008.
- [11] Wasrner, F. "Army Stepping up Its Humvee Orders for Troops in Iraq." <https://www.nytimes.com/2003/12/25/business/army-stepping-up-its-humvee-orders-for-troops-in-iraq.html>, 25 December 2003.
- [12] Blakeman, S. T., A. R. Gibbs, and J. Jeyasingam. "Study of the Mine Resistant Ambush Protected (MRAP) Vehicle Program as a Model for Rapid Defense Acquisitions." MBA professional report, Naval Postgraduate School, Monterey, CA, 2008.
- [13] Bender, D., and J. Carleone. "Explosively Formed Projectiles." *Tactical Missile Warheads*. Boulder: American Institute of Astronautics and Aeronautics, pp. 367–386, 1993.

BIOGRAPHIES

STANLEY DEFISHER serves as a mechanical engineer in the Detonation Physics and Experimental Research Branch at CCDC AC, Picatinny Arsenal, NJ, and is the current anti-armor warhead technical lead for the Joint Effectiveness Munitions Technology Program. He has worked in warheads design, fabrication, modeling, and testing for the past 17 years. Mr. DeFisher holds master's degrees in mechanical engineering and applied mathematics from Stevens Institute of Technology.

GREG STUNZENAS serves as a mechanical engineer for the Advanced Warheads Technologies Branch at CCDC AC, Picatinny Arsenal, NJ. He is currently the co-lead for shaped charge design and the principal investigator for collecting blast overpressure data for explosive breaching. He has spent over 10 years modeling various warhead and blast overpressure reduction analyses. Mr. Stunzenas holds a master's degree in mechanical engineering from Stevens Institute of Technology.

DSIAC FEATURED EXPERT - Scott Armistead



DSIAC would like to take a moment to recognize a subject matter expert who has provided users with valuable help and assistance.

SCOTT ARMISTEAD is a DSIAC senior staff engineer as well as the technical operations lead for SURVICE Engineering Company's Gulf Coast Operation. He has more than 30 years of research, development, test, and evaluation and modeling, simulation, and analysis experience in weapons integration; weapons effectiveness; weapon sensors; countermeasures/counter-countermeasure effectiveness; camouflage, concealment, and deception; and signature management. He previously served as the test manager and program engineer for the Joint Munitions Test and Evaluation Program Office; the senior engineer for the Joint Air-to-Surface Standoff Missile and Small Diameter Bomb Combined Test Flight; susceptibility lead for the Air Force Live Fire Office, and the technical

advisor for the 46th Test Wing Electro-Optical/Infrared (IR) and Millimeter-Wave (MMW) Systems Test Flight. He is experienced in technologies related to air-to-air, air-to-surface, surface-to-air, and surface-to-surface weapons; platform susceptibility/signature management; IR, visible, ultraviolet, MMW, seismic, magnetic, and acoustic sensors; and countermeasures. Mr. Armistead holds a B.S. in nuclear engineering from the University of Florida.

Years of experience: 30+ years

Expertise: weapon systems; survivability & vulnerability

Number of DSIAC publications: 27

Learn more about Scott Armistead:

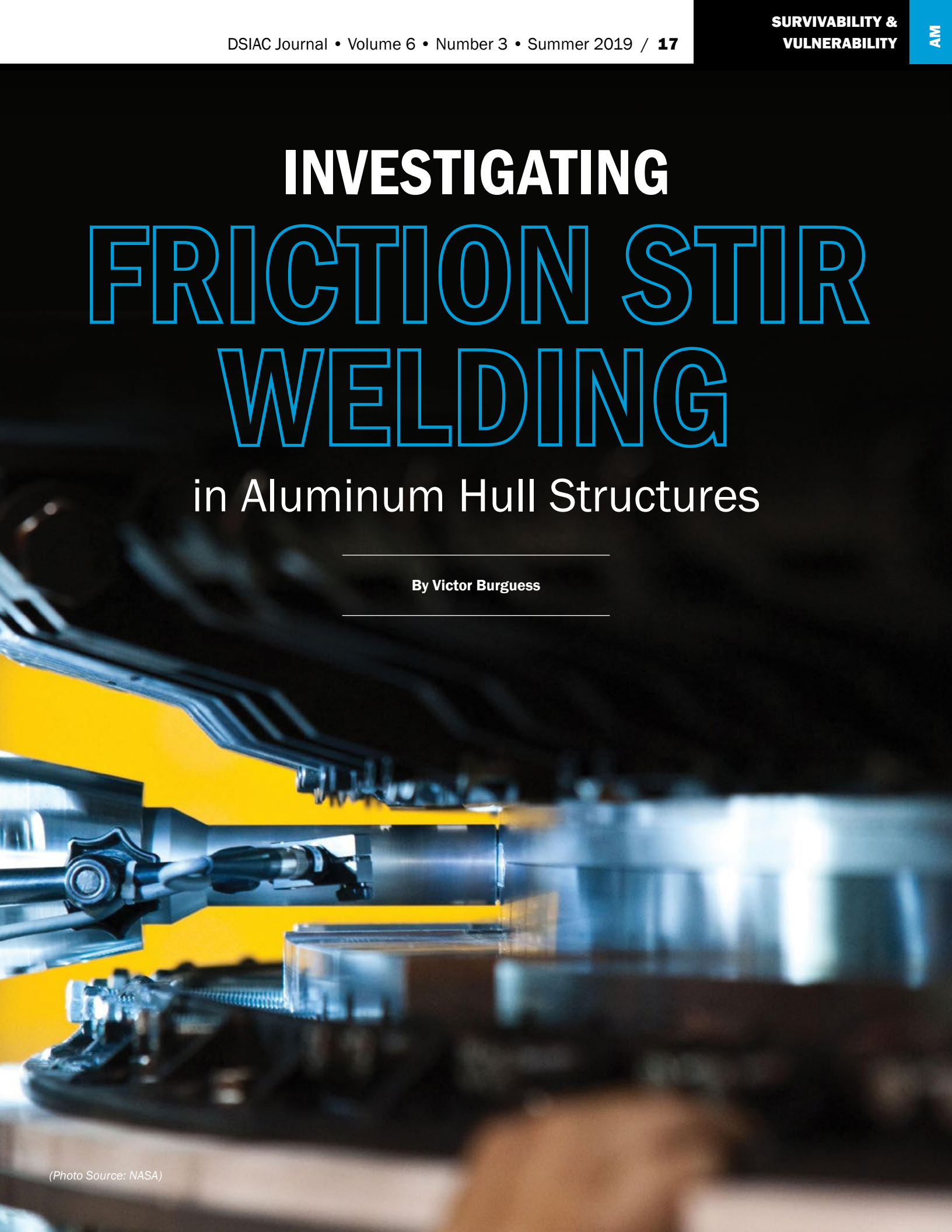
https://www.dsiac.org/resources/presenters_authors/scott-e-armistead ▶

INVESTIGATING FRICTION STIR WELDING

in Aluminum Hull Structures

By Victor Burgess

(Photo Source: NASA)



BACKGROUND

The military has shown an increased interest in developing lightweight technology solutions for current and future platforms. A large portion of this work is related to materials. New alloys are constantly being created that show benefits from two main perspectives. The first is evaluating materials that perform equivalent to the current solution at a lighter weight, and the second is materials that show an increase in performance at the same weight. A large amount of characterization must be performed to process, integrate, and evaluate in order to establish design criteria for use in military applications.

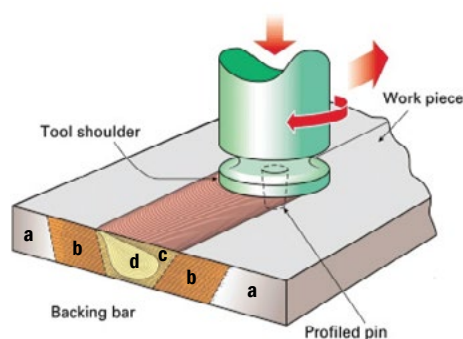
There is large interest in the U.S. Department of Defense (DoD) industry for using aluminum alloys for survivability-related applications because it has a low density when compared to current solutions and is relatively inexpensive when compared to other lightweight armor materials such as titanium. One aluminum alloy has shown a significant benefit in armor applications—2139-T8 aluminum alloy. This alloy is particularly interesting due to its ability to maintain material properties for all thicknesses. This is a significant improvement over other 2XXX and 7XXX series of high-strength aluminums.

There is a significant amount of data currently available that show 2139-T8's benefit regarding survivability applications; however, there is recent interest in its use for vehicle hull structures. This increases complexity in manufacturability and sustainment. The alloy can be gas metal arc welded (GMAW); however, the strength and elongation of the welds are 35%–55% of the base material. As an alternative, friction stir welding (FSW) can be

There is a significant amount of data currently available that show 2139-T8's benefit regarding survivability applications.

used. FSW is a solid-state welding process that uses a nonconsumable rotating tool coupled to a high-torque motor which moves along the joint of two plates, resulting in a butt weld. It is not a new technology; traditionally, the military has not utilized it during the hull manufacturing, mostly due to material selection. With the increase in emphasis for better performing technologies at lower weights comes a need to use these alloys in hull structure technologies.

Figure 1 shows a basic description of FSW. FSW has four different zones used to describe material condition. They are unaffected material, heat-affected zone (HAZ), thermomechanically-affected zone (TMAZ), and weld nugget, which is part of the TMAZ. The TMAZ and weld



- | | |
|-----------------------------|--|
| a. Unaffected material | c. Thermomechanically-affected zone (TMAZ) |
| b. Heat-affected zone (HAZ) | d. Weld nugget |

nugget are different when compared to GMAW. FSW also has a significantly smaller HAZ when compared to GMAW due to the reduction in heat input into the joint during welding. From a material preparation standpoint, there are many benefits to FSW because, in most cases, the joints can be welded with very little modification. Beveling the edges of the joint to ensure full penetration is not required; therefore, cost is reduced. Additionally, the joint tolerances tend to be significantly improved and consistent using this process.

Quasistatically, FSW has maintained 75%–85% of the base material properties in tensile strength and increased the elongation of the material in the joint by 15%–20%.

Although the material characteristics of FSW 2139-T8 aluminum are understood, additional investigation is needed for material fatigue. This is because military vehicles perform in very rigorous environments and use conditions, and the hull structure is exposed to many different loads and cycles during its life.

GOAL

The goal for this effort was to develop stress-life (S-N) curves for both base material and friction stir welded states. This would provide basic information on the rolled armor aluminum plate as well as increase or decrease performance after undergoing the solid-state welding process.

CHALLENGES

Due to the residual stress in the base plate and in the friction stir welded samples, the specimens were very difficult to machine in tolerance. Additionally, when working with aluminum, polishing the specimens to remove surface impurities that affect testing required special considerations over steel samples.

Figure 1: Description of FSW (Source: TWI Ltd.).

There are many benefits to FSW because, in most cases, the joints can be welded with very little modification.

IMPACT

Fatigue data is required when developing new platforms. This data not only shows the capability of the 2139 aluminum alloy but shows the potential benefits of FSW and its use in hull manufacturing. This provides the Army with the data required to implement new lightweight materials to modernize its current and future fleets (as demonstrated by the prototype hull shown in Figure 2).

TESTING

The testing was conducted following ISO-1143:2010 standard [1]. The machine was set up to turn off at 25 million cycles to ensure that the test was complete. An R.R. Moore Rotating Beam Test apparatus was used (shown in Figure 3, with the specimen installed).

DATA

Data was collected for the base and FSW materials for each of those cases in the longitudinal and transverse directions. The longitudinal direction was parallel to the major rolling direction, and the transverse direction perpendicular to the major rolling direction. Figure 4 shows a comparison of the base material and friction stir in the transverse direction (BMT and FT). This plot also shows three data samples that did not fail during the testing; the machine was stopped at 25 million cycles.



Figure 2: Friction Stir Welded Hull Prototype Designed by the Ground Vehicle Systems Center and Fabricated by Concurrent Technologies Corporation (Source: U.S. Army Combat Capabilities Development Command [CCDC] Ground Vehicle Systems Center [GVSC]).



Figure 3: R.R. Moore Rotating Beam Test Apparatus With the Specimen Installed (Source: CCDC GVSC).

Figure 5 shows a comparison of the base material and friction stir in the longitudinal direction (BML and FL). This plot also shows three data samples that did not fail during testing; the machine was stopped at 25 million cycles.

CONCLUSIONS

The base material proved to be relatively consistent and predictable throughout the testing. The friction stir welded material showed a larger variance

during testing. Generating data in the 10–20 million range, the cycles were difficult due to the loads selected. Some specimens would exhibit failure early, and some would continue out past 25 million cycles.

The data shows that there is a reduction in strength between the base material and friction stir welded material at low cycle fatigue; however, this trend reverses at the higher cycles. The

Stress-Life Comparison of Transverse Base Material and Friction Stir Weld

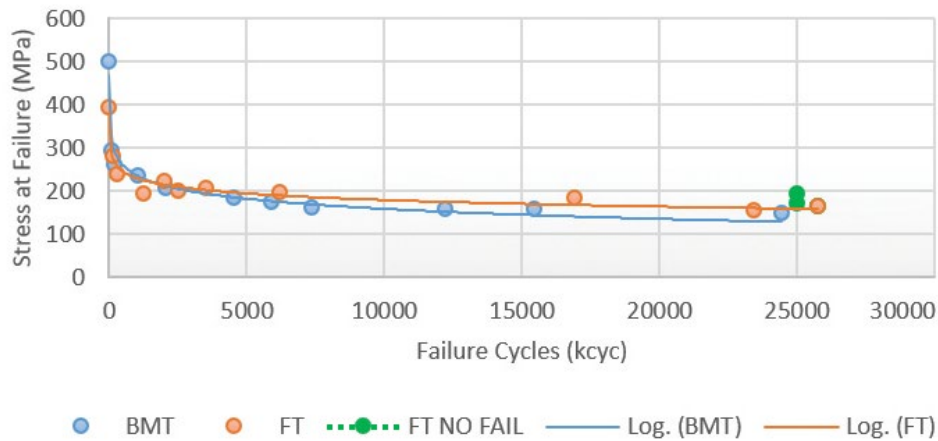


Figure 4: Stress-Life Comparison of Transverse BMT and FT Welded Material (Source: CCDC GVSC).

Stress-Life Comparison of Longitudinal Base Material and Friction Stir Weld

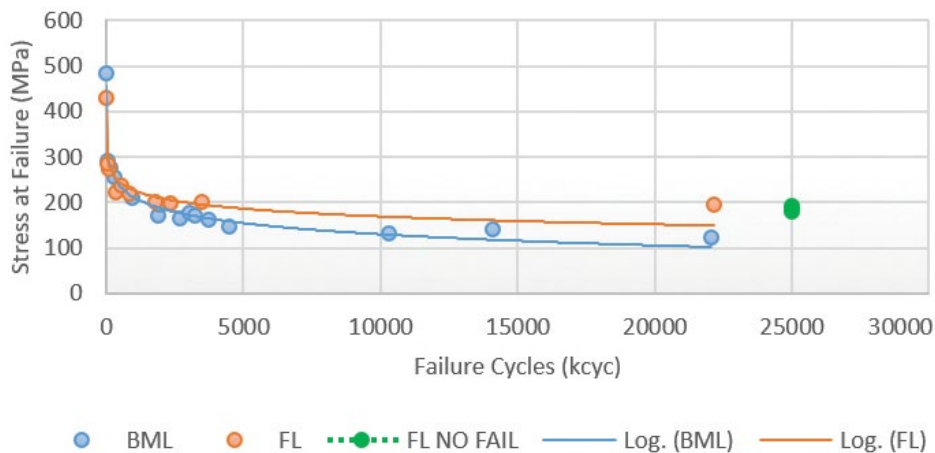


Figure 5: Stress-Life Comparison of Longitudinal BML and FL Welded Material (Source: CCDC GVSC).

friction stir welded material shows a higher failure stress at higher cycles, with an increase of 28% for transverse and 60% for longitudinal. This increase in fatigue is most likely due to the increase in ductility created by the friction stir process.

Looking at the S-N curves for the friction stir welded areas in both transverse and longitudinal directions, they appear to be very similar. This is an artifact of the stirring process where the grain boundaries of the material are altered by the FSW process. ■

ACKNOWLEDGMENTS

The author would like to thank Concurrent Technologies Corporation for the friction stir processing of the material and the fabrication of the specimens and Idaho National Laboratory for conducting the fatigue testing in compliance with ISO-1143.

BIBLIOGRAPHY

ASTM International. *Standard Practice for Statistical Analysis of Linear or Linearized Stress-Life and Strain-Life Fatigue Data*. ASTM E739-10, 2015.

Burguess, V. "Investigation in Friction Stir Welded Aluminum Alloy 2139-T8 for Hull Structure Applications," 2019.

U.S. DoD. *Armor Plate, Aluminum, Alloy 2139 Weldable & Alloy 2195 and 2060 Unwelded Applique*. MIL-DTL-32341A, 15 April 2015.

BIOGRAPHY

VICTOR BURGUESS is a research mechanical engineer at CCDC GVSC in their Ground Vehicle Survivability and Protection group. His main focus is on hull structures and underbody kits, which involves research related to materials, manufacturing, design, and testing of solutions for current and future platforms. Mr. Burgess holds a B.S. in mechanical engineering, with a minor in electrical engineering, from Kettering University.

(Photo Source: Techcon Systems)

Additively Manufactured,

Solvent-Loaded AP Composite Propellant

Printer Parameter Optimization

By Jorge Castellanos, David O. Zamor, Katherine R. Pritchett, and Christine D. Knott

INTRODUCTION

The benefit of additive manufacturing is being realized in industries where custom parts can be made when traditional manufacturing methods and economics fall short [1]. In recent years, there has been an effort to apply this technology to energetics applications, which has not seen significant technological advancement in processing for many decades [2]. The hope is to reinvigorate an aging industry vital to national defense. The best guidelines and practices governing

additive manufacturing in commercial applications do not easily translate when attempting to use them with energetic materials due to material properties and safety concerns. As such, energetic materials additive manufacturing (EMAM) is a field in which standards are not fully established [3].

Current energetic material printing solutions utilize techniques and equipment from contemporary direct ink writing (DIW) research [4–7] and the paste-dispensing industry. The feedstock is loaded into a syringe barrel, where it must dispense evenly out of a nozzle onto the desired surface. In contrast, the conventional manufacture of energetic devices, such as propellant grains, may employ the following steps

for processing: horizontal mixing, blocking and pressing, cutting, and drying.

The quality of a printed item depends on understanding the material used, with compositional and rheological information providing a great insight [5]. This can be difficult with energetics due to inherent safety concerns and the countless variations of energetic materials. If this key material information cannot be obtained, then more iterative testing is required. In these situations, it may be beneficial to create a printing parameter set not influenced by material properties. The variables that can be directly manipulated, such as material feed rate and print head movement speed, are

recorded and evaluated against material outputs, such as mass deposited and geometry. By doing so, an optimized printing parameter set can be generated in the context of the material and printing equipment.

In this research effort, a fielded propellant recipe was modified for printing optimization with a ternary solvent mixture of varying vapor pressures to support flow out of a nozzle, sustain shape integrity, and promote interlayer adhesion. A resonant acoustic mixer (RAM) was used to thoroughly mix the propellant. With mass output (g) and bead width (mm) as dependent variables, an optimal printing regime was identified and modeled, allowing print quality predictions for combinations of print-head speed (mm/s), auger speed (percent of full voltage capacity of 24 V), regulated pneumatic pressure (psi), and nozzle used (ID size and type).

METHODOLOGY

Mixing

An ammonium perchlorate (AP) composite propellant was prepared from local material stocks, comprising a polymer, plasticizer, and ternary solvent mixture. The AP used (~200 μm) was ground to <20 μm .

A solids loading of 86% by weight (wt%) AP was maintained for all mixes, keeping the plasticizer to polymer ratio at ~30/70, respectively. Solvent quantity was iteratively varied—20–50 wt%, where 35 wt% was found to be amenable for printing and taken forward for all subsequent print tests. A resonant acoustic mix of the composition is shown in Figure 1a.

Printing

A modified Fisnar F9000N robotic gantry and Fisnar RVC900N auger control box

were utilized for printing. Materials were extruded by a Techcon TS5000DMP rotary valve, using the DMP8-10, 8-pitch thread disposable auger, and Nordson Optimum SmoothFlow tapered nozzles with inner diameters (ID) of 0.41, 0.25, and 0.20 mm. The surface-to-nozzle distance was zeroed using an in-house developed accessory comprising a micrometer stage and base plate assembly connected to the extruder assembly and z-axis arm. The experimental setup is shown in Figure 2.

Optimization of Print Parameters

Bead width (mm) and mass output (g) were profiled for the AP composite propellant for a given nozzle ID (mm), pressure (psi), print-head speed (mm/s), and auger speed (%V) to gauge optimal printer settings. Output pressures tested were 50, 75, and 85 psi. Print-head speeds tested were 1–20 mm/s at 2-step increments. The auger speeds tested were from 10 %V to 100 %V at 10-step increments. The z-height was set to approximately 88% of the nozzles' ID. AP composite propellant



Figure 1: (a) RAM of AP Composite Propellant Feedstock Used and (b) Mix Consistency (Source: Naval Surface Warfare Center [NSWC]-IHEODTD).

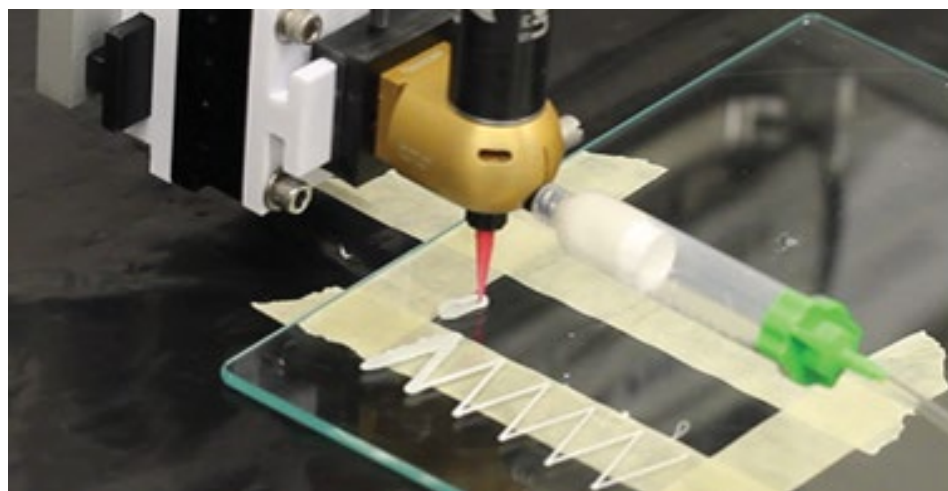


Figure 2: Gantry Setup With a Techcon TS5000DMP Rotary Valve for Printing With Inert and Energetic Materials (Source: NSWC-IHEODTD).

samples were printed using a toolpath program producing zig-zag lines with 11 different 30-mm line segments, each representing a combination of nozzle size, pressure, print-head speed, and auger speed (see Figure 2). To identify the key cause-effect relationships amongst the variables, a visual assessment of print quality was made. The segments' bead width, height, and mass were recorded once dried. Origin(Pro) 2018, Version 95E was used for generating surface plots and data analysis.

RESULTS AND DISCUSSION

A commercial modeling compound was chosen for initial printing tests, as it mimicked the RAM-generated propellant feedstock (Figure 1b), and to provide an initial printing parameter baseline (Figure 3).

After the prints with the modeling compound, worked parameters were used for initial tests using the propellant feedstock, with limited success (Figure 4a). Clogging issues caused erratic flow during printing, leading to failures (Figure 4b). These clogs could be seen as small agglomerate clumps becoming lodged in the nozzle, preventing even flow (Figure 4c). This would even cause the nozzle to unscrew itself from the auger's feed path (Figure 4d).

Initial line tests were done by printing four different line segments at a time, which was eventually changed to a zig-zag pattern to easily capture more data points (Figure 5). Qualitatively, an ideal line was considered to be straight, showed little variation in bead width, and adhered well to the substrate. Several undesirable morphological anomalies were observed, such as discontinuity in bead width due to overextrusion and underextrusion. Periodic wave-like patterns in the line segments could be

due to the design of the auger, thus needing further investigation.

The test series was successfully completed under all conditions for the 0.41-mm nozzle but was not completed for the 0.20-mm and 0.25-mm nozzles due to clogging. It was postulated that agglomerates of AP caused the clogging observed in the smaller ID nozzles after

the orifice was restricted by accumulated material. In addition, this might be due to the particle size distribution inherent to the ground AP. In the future, the presence of agglomerates will be closely monitored during feedstock preparation to ensure elimination.

Mass and bead width decreased exponentially with increasing print head



Figure 3: Iterations of Initial Prints Using a Commercial Modeling Compound (Source: NSW-IHEODTD).

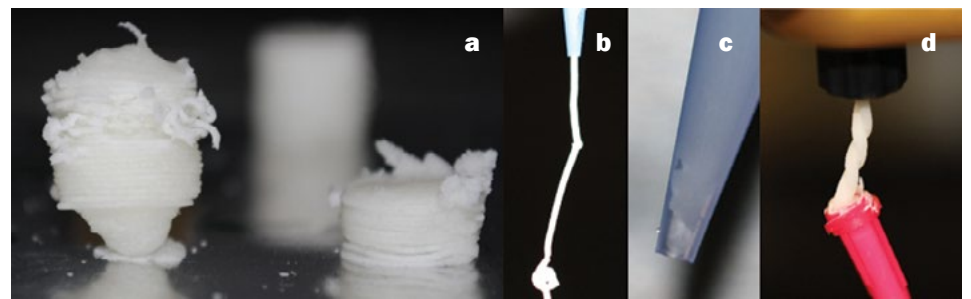


Figure 4: Issues Encountered During Initial AP Feedstock Printing Tests: (a) Over and Under Extrusion, (b) Erratic Flow, (c) Clogging, and (d) Nozzle and Auger Decoupling (Source: NSW-IHEODTD).

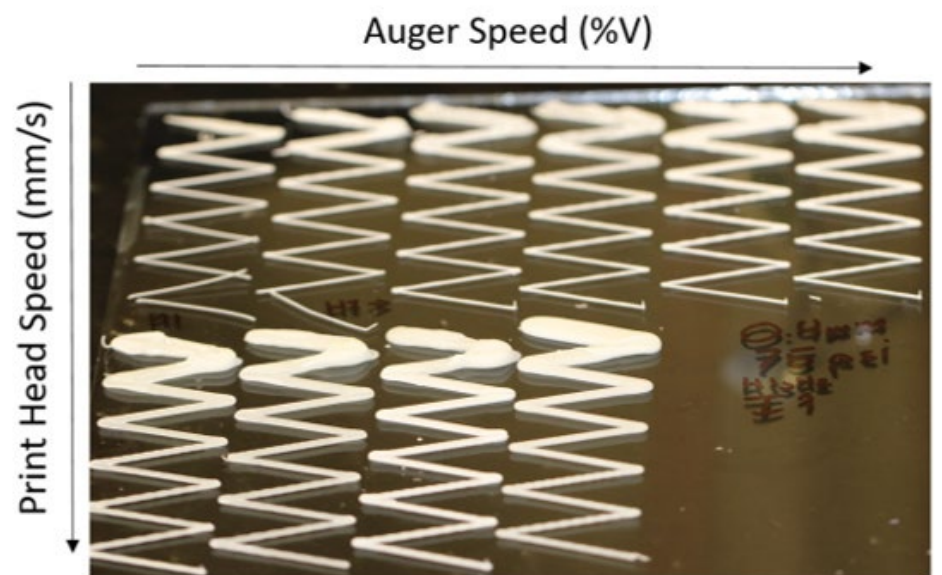


Figure 5: Print Optimization Zig-Zag Test Series (0.41-mm Nozzle, 75 psi), With a 30° Angle Between Each Line Segment (Source: NSW-IHEODTD).

speed. This identified the first ideal parameter combination, where one variable's effect was insignificant with a change in another—the mass was relatively unchanged at higher print-head speeds. Bead width, however, was more affected by changes to auger speed.

To understand the effect of pressure on printing with an auger attachment, a mass flow rate vs. auger speed plot was generated for each pressure. As expected, the data showed a linear increase in mass flow over the range of lower auger speeds for all pressures. However, at the midpoint in the auger speed range, a dip in mass flow rate was noticed, followed by erratic flow rates at higher auger speeds. This behavior may be due to either the non-Newtonian characteristics of the fluid, a deviation of the extruder motor function from control input, material not being introduced into the nozzle rapidly enough at higher auger speeds (thereby, potentially generating voids in the print), or some combination of these factors. A linear operating range between 10 %V and 50 %V was established for near-term efforts to print propellant grain geometries. An auger speed of 40 %V and pressure of 75 psi were chosen as optimal settings moving forward.

To illustrate these discussion points, the data was represented as a surface plot using a global representation of mass or bead width related to changes to auger speed and print-head speed. The aforementioned dip in extrusion performance manifests as a trough running through the middle of the plot. Ideal quality line segment prints were observed at combinations of higher print-head speeds and lower auger speeds. This particular region could be modeled as a simplified plane equation (1), where z is either mass or bead width in grams or millimeters, z_0 is a constant

The data showed a linear increase in mass flow over the range of lower auger speeds for all pressures.

in grams or millimeters, and a and b are slopes in the XZ ($\Delta\text{mass}/\Delta\text{print-head speed}$ or $\Delta\text{bead width}/\Delta\text{print-head speed}$) and YZ planes ($\Delta\text{mass}/\Delta\text{auger speed}$ or $\Delta\text{bead width}/\Delta\text{auger speed}$).

$$z = z_0 + a(x) + b(y). \quad (1)$$

The obtained slopes indicated that both mass and bead width were more sensitive to changes in print-head speed than auger speed, approximately 4x for mass and 2x for bead width.

A propellant grain geometry (approximately a cylinder the size of a 0.40-mm round) was therefore printed using parameters generated from the aforementioned ideal region. No grains could be printed to completion using the smaller nozzle sizes, exemplifying the issue with clogging (Figure 6).

When using the larger 0.41-mm nozzle size, the grain geometry printed to completion; however, there were several defects. The exterior was nonuniform,

and each layer's cross section exhibited gaps between shells. Seam points were markedly exaggerated. These "pimple-like" surface defects, shown in Figure 7a, were thought to be a result of overextrusion at the start-stop points between layers. A retraction time was incorporated in the next iteration to prevent material buildup at each layer change. The auger speed was slightly increased by 1–3 %V in an attempt to fill the gaps between shells due to underextrusion. These changes improved the quality of the print, as seen in Figure 7b.

Additional grains were printed using these parameters. Each print had similar quality and appearance, providing confidence in the parameter down-selection methodology (Figure 8). The dimensions were measured immediately after printing and once when fully dry. There was a small reduction in height and diameter due to solvent evaporation, which can be accounted for in future prints. Also, the density of the printed grains was lower than the traditional baseline fielded article. The lack of bonding between shells could be a symptom of underextrusion, contributing to the issue of lower density.

CONCLUSIONS

Optimal starting point parameters for producing small propellant grains



Figure 6: Failed Grain Prints Using Smaller Nozzle Sizes Due to Clogging (Source: NSWC-IHEODTD).

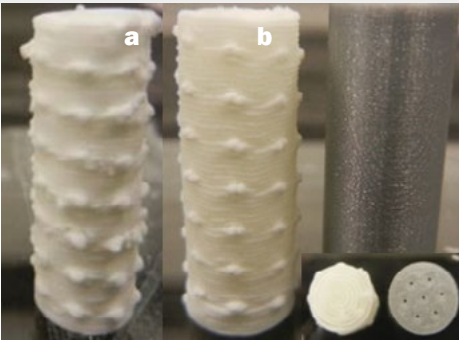


Figure 7: Progressions of AP Composite Propellant Grain Geometries: (a) Initial Print and (b) Improved Print Alongside Fused Filament Fabrication Print (Inset: Top-Down View) (Source: NSWC-IHEODTD).



Figure 8: Repeated Grain Prints Utilizing Optimized Parameters With Retraction Time (Source: NSWC-IHEODTD).

By measuring and analyzing bead width and mass output, printing parameters could be down-selected and used to print grain geometries in free form.

via three-dimensional (3-D)-DIW were found, and a method to obtain them was demonstrated. By measuring and analyzing bead width and mass output, printing parameters could be down-selected and used to print grain geometries in free form. This methodology for acquiring printing envelopes may be used for other materials using 3-D-DIW in the future. The acquired parameters could also be used to improve the output of a conventional toolpath generation software. One such parameter shown to reduce surface defects was retraction time; however, this needs further investigation. The conclusions of this work are expected to support follow-on efforts to print grain geometries with

perforations, eliminate defects, and evaluate performance. ■

ACKNOWLEDGMENTS

This research was sponsored by the Energetics Manufacturing Technology Center ManTech Program and Cartridge-Actuated Device/Propellant-Actuated Device Joint Program Office (PMA-201). The authors thank the Energetics Manufacturing Department at NSWC-IHEODTD for supplying raw materials and grinding the ammonium perchlorate.

REFERENCES

- [1] The Economist. "3D Printers Start to Build Factories of the Future," 29 June 2017. <https://www.economist.com/briefing/2017/06/29/3d-printers-start-to-build-factories-of-the-future>, accessed 13 March 2019.
- [2] DeFusco, A. "Rocket Propulsion Industrial Base: A Status Report." *DSIAC Journal*, vol. 4, no. 1, pp. 11–16, 2017.
- [3] Ruz-Nuglo, F., L. Groven, and J. A. Puszynski. "Additive Manufacturing for Energetic Components and Materials." In the 50th AIAA/ASME/SAE/ASEE Joint Propulsion Conference, Cleveland, OH, 2014.
- [4] Feilden, E., C. Ferraro, Q. Zhang, E. García-Tuñón, E. D'Elia, F. Giuliani, L. Vandepierre, and E. Saiz. "3D Printing Bioinspired Ceramic Composites." *Scientific Reports*, 23 October 2017.
- [5] Jakus, A. E., K. D. Koube, N. R. Geisendor, and R. N. Shah. "Robust and Elastic Lunar and Martian Structures From 3D-Printed Regolith Inks." *Scientific Reports*, 2017.
- [6] M'Barki, A., L. Bocquet, and A. Stevenson. "Linking Rheology and Printability for Dense and Strong Ceramics by Direct Ink Writing." *Scientific Reports*, 20 July 2017.
- [7] Pattinson, S. W., and J. A. Hart. "Additive Manufacturing of Cellulosic Materials With Robust Mechanics and Antimicrobial Functionality." *Advanced Materials Technologies*, vol. 2, no. 4, p. 1600084, 2017.

BIOGRAPHIES

JORGE CASTELLANOS is a chemist at NSWC-IHEODTD, where he has been actively involved in multiple projects for the U.S. Navy in EMAM. Dr. Castellanos obtained a B.S. in biomolecular science, with a concentration in chemistry from Polytechnic Institute of NYU, and a Ph.D. in applied chemistry from the University of Puerto Rico at Mayagüez.

DAVID O. ZAMOR is a chemical engineer at NSWC-IHEODTD, where he researches additive manufacturing using energetic materials. He first worked as an in-service engineer for the CAD/PAD Department and then transferred to the Research and Development Department to pursue research in additive manufacturing using energetic and other nonstandard manufacturing materials. Mr. Zamor holds a bachelor's degree in chemical engineering from Virginia Tech.

KATHERINE R. PRITCHETT is a physicist at UK Defense Science & Technology Laboratory (dstl) within the Energetic Technology Group. She has been involved in multiple projects involving energetics, including EOD research and additive manufacture of energetic materials. Ms. Pritchett obtained a master's degree in astrophysics from University College London.

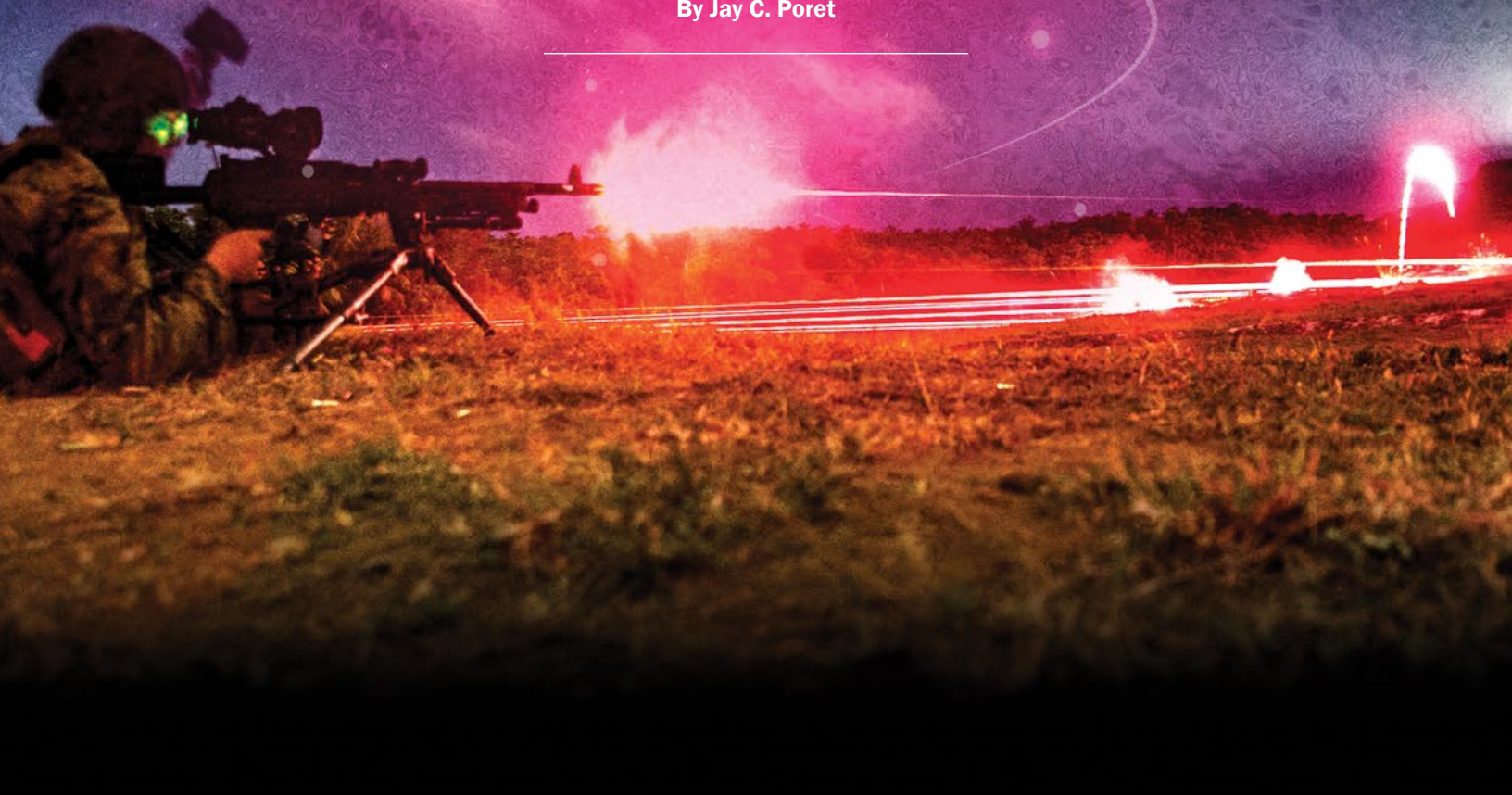
CHRISTINE D. KNOTT is a chemical engineer at NSWC-IHEODTD, where she serves as a gun propellant formulations and process development engineer. She is responsible for developing formulations, mostly nitramine and nitrocellulose-based, where she is regarded as a nationally recognized expert. She is also responsible for processing methods for most new propellants used in gun systems for the U.S. Navy and Army and for gas generators and various other Navy applications. Ms. Knott holds a bachelor's degree in chemical engineering and chemistry from the University of Maryland, Baltimore County.

(Photo Source: U.S Marine Corps)

A Multisensor System for Measuring the Light
Output and Velocity of Live-Fired, Red Light-Emitting

PYROTECHNIC TRACERS

By Jay C. Poret



SUMMARY

This article describes a multisensor system for measuring the light output and ballistic velocity of pyrotechnic tracers fired from a weapon. The sensors are composed of unbiased silicon photodetectors coupled to 75-mm-diameter aspheric glass lenses. A narrow bandpass filter (center wavelength [CWL] = 665 nm and bandpass = 30 nm) is placed in the optical path, allowing the tracer's peak spectral emission lines to pass through to the detector yet minimizing the amount of ambient light. This allows light emitted from fired tracers to be measured in all lighting conditions.

INTRODUCTION

Soldiers have long used light emitted from tracers to adjust their weapons to ensure successive rounds strike their intended targets. Tracers are typically packed in a 4-to-1 configuration in automated weapon systems—one tracer for every four ball rounds (nontracer) [1]. One of the most common tracers used by the U.S. military is the red light-emitting tracer, which is used in many different calibers (i.e., 5.56 mm, 7.62 mm, and .50 caliber).

Most tracer manufacturing facilities are high-rate production facilities producing thousands of tracers per hour. As with most military munitions, tracers are produced in lots, and a small number of them are fired on a test range to ensure they meet military specifications. In the United States, tracers are tested at night by firing a specified number of rounds, and downrange human observers score the visibility of the tracer.

To evaluate the 7.62-mm M62 tracer round, human observers are placed behind the weapon at 14 m (15 yd), 91 m (100 yd), and 777 m (850 yd) from the muzzle of the weapon. Each station is located 69 m (75 yd) perpendicular to

the firing line. Observers visually score how “well” the tracer performs. For example, if an observer cannot see the tracer, it is classified as “blind.” If the tracer's flight is erratic, it is classified as “erratic.” The military specification for the cartridge stipulates how many defects (i.e., blinds, muzzle flashes, and erratic flights) are allowed for a production lot to pass the acceptance test. No optics or instrumentation are used in these measurements—only human observers reporting how well they see the tracers. This measurement is very subjective and will vary greatly from person to person.

While spinning a tracer creates an aerodynamic environment that is more realistic than a static burn, it still does not adequately replicate the conditions the projectile experiences when fired out of a weapon.

Human vision and visual perception have been extensively studied for many years. Many models have been developed that describe how humans perceive color and brightness [2]. Over the years, studies have shown that different people will perceive luminous events differently. For instance, one person might describe a luminous object as a deep red while another person might perceive the same light source as a deep pink. The cone's (color) and rod's (low-light intensity) cells of the eye degrade with age, influencing how people perceive color. Additionally, as people get older, their pupils lose their

ability to expand; this limits their ability to differentiate changes in ambient light levels [3].

Over the years, military researchers have developed laboratory techniques for evaluating the light output of pyrotechnic tracers. One of the simplest ways is to statically ignite a tracer in a fixed block (or holder) and measure the light output with a light detector. While this is a quick method for assessing a tracer's light output, it does not yield a realistic measurement of the tracer's light output or burn time when fired from a weapon.

A better way to simulate a fired tracer is to ignite a tracer inside a high-rate spin fixture. Researchers have developed fixtures for spinning tracers and measuring the light output at high rotational velocity [4]. Buc et al. describe spinning developmental tracers at 21K rpm (and blowing air along the spin axis) so they could measure the tracer's light output at non-static conditions [5]. Briere described a turbine-based spin apparatus that can spin tracers up to 300K rpm [6]. In this laboratory, tracers have been spun up to 80K rpm using a pneumatic-based spin device.

While spinning a tracer creates an aerodynamic environment that is more realistic than a static burn, it still does not adequately replicate the conditions the projectile experiences when fired out of a weapon. Tracers spin much faster when fired out of a weapon than what is easily achievable in a laboratory fixture. For example, the calculated rotational velocity of the M62 tracer is around 160K rpm. The calculated projectile spin rate depends on the barrel length and number of grooves per inch inside the gun barrel [7]. Additionally, the projectile spin rate creates aerodynamic forces on the tail of a projectile that affects the burn rate and slag removal (produced from the

burning tracer) not easily recreated in the laboratory.

Measuring the light output from a static or spun tracer in a laboratory setting is relatively straightforward. Measurement devices are aimed at either a static or spinning tracer, and the light output is measured with either a single-element detector or charge-coupled silicon device (for spectral measurements). As an example, Brier used a photometer and a broadband radiometer to obtain both eye weighted photometric daytime response measurements and broadband radiometric measurements on tracers spun at different spin rates.

But how do we measure the light output from a live-fired tracer traveling several thousand feet per second? One of the first quantitative methods for measuring the light output from *fired* tracers was developed by Reilly [8]. In this system, 8-bit video cameras were placed at each of the observation stations (previously described) and linked together with gigabit Ethernet to a central processing station. The data consist of a single video frame with a streaked image. To establish thresholds for passing and failing, two different threshold criteria were developed—the average pixel value and the number of pixels detected within an image. Due to the configuration of this system, measurements were only performed at night.

In this article, a system is demonstrated using low cost commercial-off-the-shelf (COTS) components. Using large area, filtered silicon photodetectors combined with programmable transimpedance amplifiers allows the tracer's optical emissions to be measured at different ambient light levels. Analog/digital converters allow data from remote detectors (over optical fiber) positioned along the line of fire (LOF) to be collected at a central processing station. Since

This is the first system that can simultaneously measure *both* the tracer's light output and average velocity of a fired tracer projectile using only the light emitted from the tracer.

the output from the detectors is collected simultaneously, the average tracer velocity between adjacent detectors is easily measured. This is the first system that can simultaneously measure *both* the tracer's light output and average velocity of a fired tracer projectile using only the light emitted from the tracer.

EXPERIMENTS

System Schematic

Figure 1 shows the overall layout of the system. The dotted lines represent optical fibers, and solid lines represent coaxial cable. A Mann barrel system was used to fire 7.62-mm M62 red light-emitting tracers. The detectors were placed ~4.3 m perpendicular from the tracer's LOF. The control module and first silicon detector

were placed 50 m from the barrel, the second silicon detector module 150 m from the barrel, and the third silicon detector 250 m from the barrel. The 50-m detector's transimpedance output was directly connected to the data card in the control module by a 50-ohm coaxial cable while duplex, single-mode fiber optic cables connected the 150- and 250-m detector stations to the control module (located at 50 m). The control module was connected to the computer station by an Ethernet cable. An acoustic trigger (Kapture Group MD1505) was used to send a 5-V transistor-transistor logic pulse when the gun was fired to trigger the data collection system.

Detectors

The detectors used in this system were 100 mm² unbiased silicon detectors made by Thorlabs (SM1PD1A). Light was coupled into the detector using a Thorlabs 75-mm-diameter, antireflection, coated, aspheric condenser lens with a focal length of 60 mm (ACL7560U-A). An Omega Optical bandpass filter with a CWL of 665 nm and bandpass of 30 nm was placed in front of the detector. The lens detector distance was optimized by using a white light source placed 2 m away to aid in setting the optimal distance between the lens and the detector and produce the smallest spot size onto the active area of the photodetector.

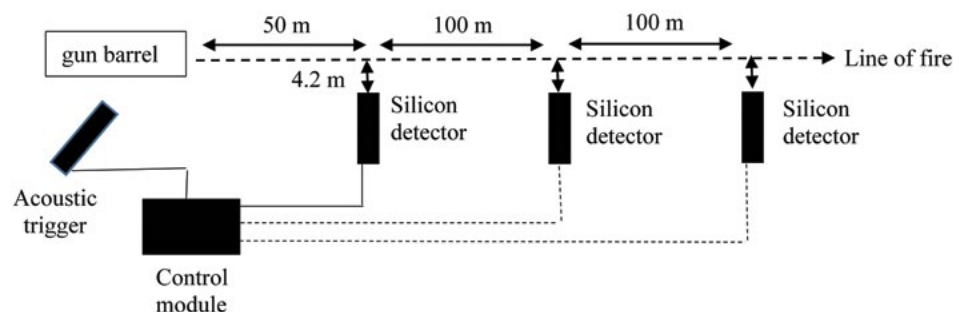


Figure 1: Overall Range Schematic of the Tracer Measurement System (Source: J. Poret).

Amplification

The current output from the detectors was converted to voltage using two different transimpedance amplifiers. The transimpedance amplifier placed at the 50-m detector station was a DL Instruments 1211 amplifier. Stanford SRS570 transimpedance amplifiers were used at the 150- and 250-m detector station due to their built-in RS232 interface, which allowed the amplifier setting to be remotely controlled by RS232 serial commands.

Amplifier Control and Voltage Measurement From the 150- and 250-m Detector Stations

As described, SRS570 amplifiers were used in the 150- and 250-m detector stations. At these distances, Ethernet, USB, and coaxial cables were impractical for sending signals over hundreds of meters. To send and receive signals between the detector stations and the main station, signals were sent over single-mode optical fiber cables using media converters. Serial media converters (Blackbox ME662A-SST) were used to send serial commands to the SRS570 amplifier so gain and voltage offset could be set remotely from the control computer. The transimpedance amplifier's voltage output was converted to an optical signal and sent over a second single-mode optical fiber with a 14-bit optical/electrical converter (Terahertz Imaging LTX5510-R-1310-14). Figure 2 shows a schematic of the (a) control module and (b) 150- and 250-m detector modules. Wire lines drawn with a dotted line represent a single-mode optical fiber, while solid lines represent copper coaxial cables. Arrows in both diagrams indicate signal direction between components. All of the amplifier outputs were collected at 75 kS/s with a simultaneously sampling 16-bit data card (National Instruments NI-9215)

and processed with in-house developed acquisition software.

Detector Calibration and Signal Latency Measurement

To calibrate the detectors, a three-lamp integrating sphere (Labsphere) with an integrated spectrometer was used to calibrate each of the filtered detectors. The detectors were positioned 2.7 m from the integrating sphere's exit aperture (10.2-cm diameter), and six different light levels were used to calibrate each detector. Different light levels were generated using a variable aperture in front of one of the lamps and switching off the other two lamps as required to generate lower light levels. The calibration factor for each detector was generated by taking the slope of the irradiance vs. output voltage (at the amplifier gain used during

the measurement) from each detector/transimpedance amplifier module.

Another experiment was performed to measure the latency, or time lag, of the detectors connected by optical fiber to the command module. A modulated red LED (Thorlabs M623L3 and DC2200) was used to generate a square wave from which a time shift in the detector's voltage output could be measured. The detector was connected to one of the SRS amplifiers, and the voltage output from the amplified detector was split into two using a BNC-T connector. One leg was routed directly to one channel of a four-channel, 350-MHz oscilloscope (Teledyne Lecroy HDO4034), and the other leg was routed into the fiber-based system. The output from the fiber system was routed into a second channel of the oscilloscope.

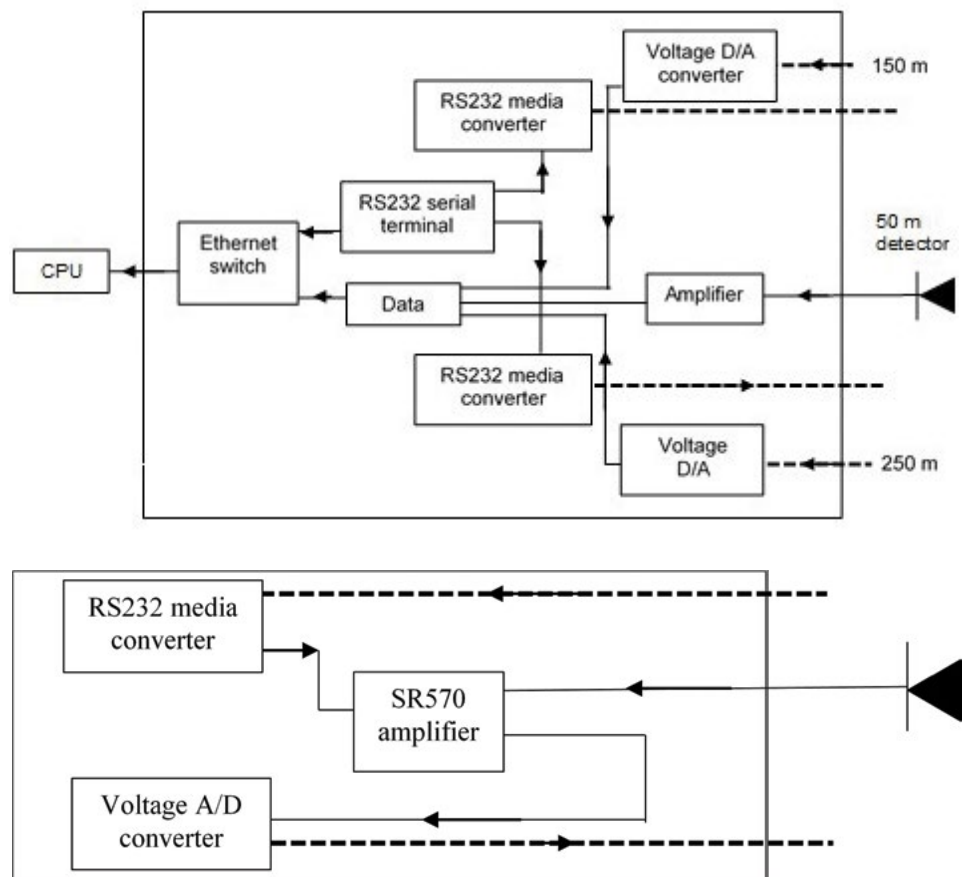


Figure 2: Diagrams of the Control and Remote Modules (Source: J. Poret).

The time delay between the two legs was calculated using the oscilloscope's skew function and measured $\sim 1.8 \mu\text{s}$. Measurements were performed at square pulse modulation frequencies of 500 Hz and 10 kHz, and the same time delay was obtained for the skew measured at both frequencies.

Spectrometer and Spin Device

An Ocean Optics HR2000+ spectrometer with a 400- μm core fiber was used to collect the emission spectrum of the static and spun tracers. The wavelength calibration of the spectrometer was performed with a Hg-Ar light source, and the radiometric calibration of the spectrometer/fiber was calibrated with a LS-1-Cal light source. The tracers were spun on an in-house designed, pneumatic turbine system.

RESULTS AND DISCUSSION

The need for a responsive, quantitative system that can accurately determine the intensity of fired tracers was the driving force behind this developmental effort. Originally, this system was developed for night measurements but was expanded to include daytime measurements to enhance the system's functionality. Because tracers are only tested at night, developing a system that can work day and night would be advantageous to manufacturers since it would allow testing at any time. Additionally, range operations would be safer since daytime testing potentially reduces the possibility of accidents that have a higher probability of occurring at night.

One of the key aspects in developing a system that works in the daytime is understanding the tracer's spectral emission. Red light-emitting pyrotechnic compositions are typically comprised of

Because tracers are only tested at night, developing a system that can work day and night would be advantageous to manufacturers since it would allow testing at any time.

strontium nitrate, polyvinyl chloride (a chlorine donor), and magnesium. In a tracer projectile, the tracer composition is pressed into a small cavity in the back of the projectile, followed by the ignition mixture. When the cartridge's primer is struck by the firing pin of the weapon, the hot particles emitted by the primer ignite the propellant. This, in turn, ignites the ignition mixture and the tracer mixture, causing the tracer composition to emit red light.

The red light-emitting species, SrCl, is a metastable radical that is a very efficient red light emitter [9]. Figure 3 shows the emission spectrum of an unspun M62

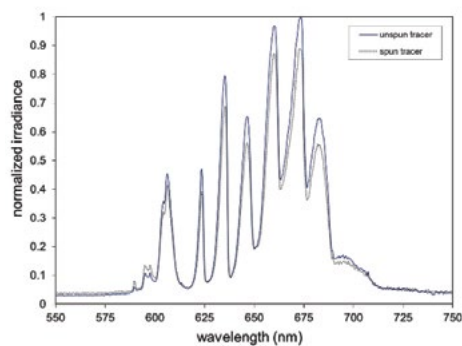


Figure 3: Normalized Spectral Irradiance of a Static and Spun (41.3K rpm) Strontium-Based, Red Light-Emitting M62 Tracer (Source: J. Poret).

tracer and M62 tracer spun at 41.3K rpm. The spectrum is normalized to the peak emission line occurring at 674 nm. Note that the position of the spectral peaks do not shift when a tracer is spun. In general, spinning a tracer will typically increase the burn rate and decrease the amount of light emitted from a tracer [10, 11].

Figure 4 shows the solar spectrum emitted by the sun over the tracer's spectral range. The maximum irradiance was normalized to the peak irradiance value within the 500–700-nm wavelength range [12]. The sun's intense emission in the spectral range of silicon detectors (300–1000 nm) is why daytime visible light measurements of pyrotechnics is very difficult, especially when large-diameter aspheric lenses are coupled to large-area silicon detectors.

Early in this program, when the detector modules were tested in full sun conditions (without the narrow bandpass filter), measuring the tracer's emitted light at high amplifier gains (10^5 A/V and 10^6 A/V) was very difficult due to the ambient light levels normally present during daytime measurements. The resultant output voltage from the amplifier would almost exceed the voltage range of the data card before the tracers were fired from the weapon.

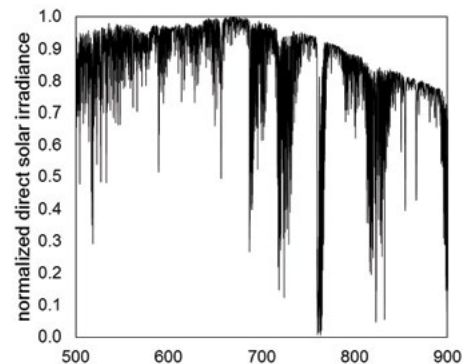


Figure 4: Normalized Direct Solar Irradiance vs. Wavelength Range of the Silicon Detectors (Source: J. Poret).

To reduce the amount of ambient light incident on the detector, a COTS narrow bandpass filter was inserted into the optical path of the detector module. COTS filters with different CWLs (and bandpasses) were evaluated by comparing the integrated areas of the M62 spectral emission for each bandpass of the available filters. Initial live testing showed that filters with narrow bandpasses (yet still within the M62 tracer's spectral emission) were better suited for daytime measurements due to lower levels of ambient light incident onto the detector.

A filter with a center 665-nm wavelength and 30-nm bandpass was inserted into the optical path since it had the largest integrated area compared to the other evaluated filters. Figure 5 shows the filter's bandpass superimposed onto the normalized spectral emission of the tracer. This filter allows the tracer's primary emission lines to pass through the filter, yet significantly reduce the amount of broadband light (normally present during daytime measurements) from being collected by the aspheric lens and focusing onto the active area of the detector.

Another advantage of this multidetector concept is the ability to calculate the average ballistic velocity between adjacent detectors. Traditionally, a tracer's ballistic

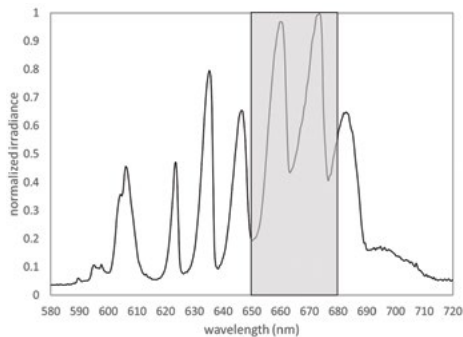


Figure 5: Plot Showing the Spectral Window of the 665-nm Bandpass Filter Superimposed on the Tracer's Spectral Emission (From Figure 3) (Source: J. Poret).

Another advantage of this multidetector concept is the ability to calculate the average ballistic velocity between adjacent detectors.

velocity is calculated by firing the tracer between two laser screens with a known distance and measuring the projectile's time of flight between the screens. Using the well-known relationship for velocity,

$$v = \frac{\Delta X}{\Delta t}, \quad (1)$$

where v is average velocity, ΔX is the distance between the two laser screens, and Δt is the projectile's time of flight between the two laser screens. The tracer's velocity is easily calculated.

Likewise, the tracer's velocity between adjacent pairs of detectors can also be calculated. Figure 6 shows a plot of a tracer fired in the daytime, with three detectors collecting simultaneous data. The three amplifier voltage outputs are collected at the same time. The top plot is the output from the detector at 50 m, the

middle plot is the detector at 150 m, and the bottom plot is the detector positioned at 250 m. All three plots use the same x- and y-axis units. If one uses the time difference between the *peak* irradiance from each detector, the average ballistic velocity between detectors 1 and 2 and detectors 2 and 3 can be calculated. For this particular tracer, the average velocity between detectors 1 and 2 was 762 m/s and 695 m/s between detectors 2 and 3. Based on publicly available data for the M62 tracers, the velocity measured between detectors 1 and 2 is very close to the published value of 814 m/s (measured 24 m from the gun barrel) [13].

Figures 7 and 8 show other examples of how this system can detect tracers that did not emit light or tracers that emitted low levels of light. Figure 7 shows a "blind" tracer. Note that the tracer irradiance in Figure 8, potentially a dim tracer, is extremely low compared to the tracer shown in Figure 6. Differences in tracer output can be caused by a number of manufacturing variables such as incorrect consolidation pressure, varying dwell time, and variation in particle size of fuel and oxidizers used in the igniter and tracer compositions.

Another important aspect is the detector field of view (FOV). The detector's angular field of view (AFOV) for a lens coupled to

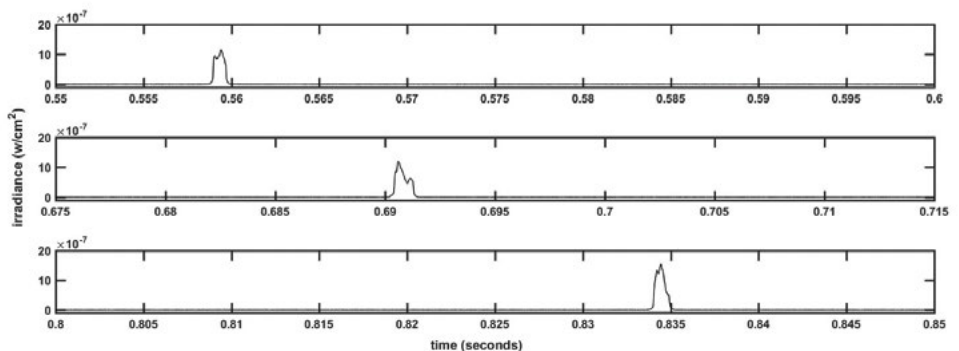


Figure 6: Irradiance vs. Time for a Daytime-Fired Tracer (Source: J. Poret).

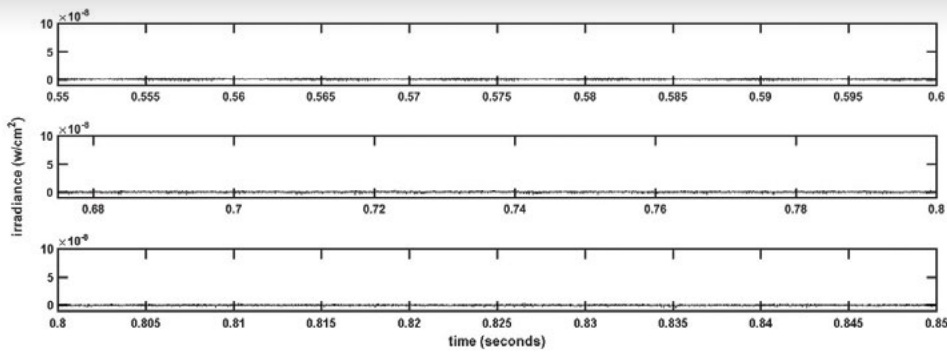


Figure 7: Irradiance vs. Time for a Blind Tracer Fired at Dusk (Source: J. Poret).

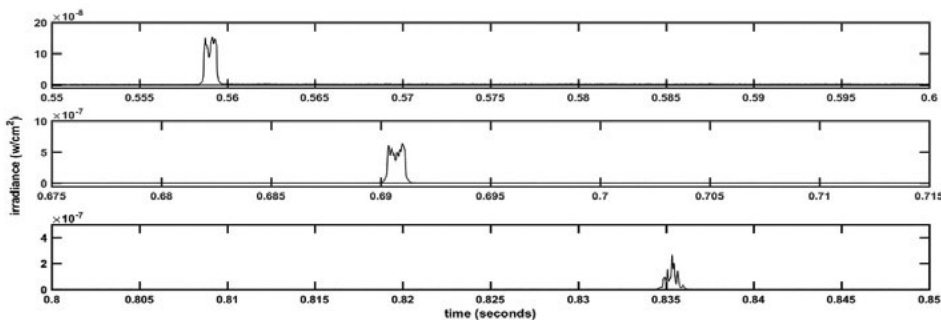


Figure 8: Irradiance vs. Time for a Potentially "Dim" Tracer Fired in the Daytime (Source: J. Poret).

a detector can be calculated using the following equation:

$$AFOV = 2 \tan^{-1} \left(\frac{h}{2f} \right), \quad (2)$$

where h is the height (diameter) of the detector and f is the focal length of the lens [14]. Using the detector's height and focal length of the lens yields an AFOV of 9.5° . In these measurements, the total FOV the detector sees at 4.3 m from the LOF is approximately 0.71 m. As long as the detector's spacing is larger than the detector's FOV, there will be no overlap between adjacent detectors.

In this article, a system has been demonstrated that can effectively "map" out a tracer's irradiance and velocity profile as a function of range distance along the LOF using multiple silicon detectors coupled to large-diameter aspheric lenses (with an appropriate bandpass filter). This system is expandable as the number of detectors in a system will be limited by the

data collection system, distance between detector modules (fiber length from detector station to control module), and the detector's FOV. Latency effects due to the use of analog-to-digital (A/D) converters over optical fibers will have minimal effect on the overall time measurement since the latency time delay corresponds to microseconds and our measurements correspond to tenths of seconds (Figures 6 and 8).

The use of aspheric lenses is also important as large-area aspheric lenses will enable more efficient light collection than other types of lenses (i.e., plano-convex). For example, aspheric lenses can typically be purchased with lower focal lengths than plano-convex lenses of similar diameter, therefore allowing larger FOVs for a given detector-lens combination. Additionally, aspheric lenses will have less spherical aberration, resulting in smaller spot sizes and less blurring than other

The use of aspheric lenses is also important as large-area aspheric lenses will enable more efficient light collection than other types of lenses.

types of lenses. The large area aspheric lens is also important for collecting light from dim sources since larger lenses will collect more light than smaller lenses.

This system is vastly different than the camera system developed by Reilly [8]. In their system, the number of pixels and pixel values is analyzed on a single frame per fired tracer. In this system, data are *continuously* collected by the detectors (once triggered). The data generated by each detector are sampled at the same time since a simultaneously sampling data card is used. It is possible to observe unusual tracer behavior (i.e., fragmentation) if the event occurs within the detector's FOV as a function of time due to the high data collection rate of this system. Tracers with low and high light output are easily distinguished from one another. Additionally, the average tracer velocity can be measured for fired tracers by using multiple pairs of detectors.

CONCLUSIONS

A new method of measuring both the tracer's irradiance and its velocity from the same fired projectile has been demonstrated. Using large-area silicon detectors coupled with large-diameter aspheric lenses enables detecting light emitted from live-fired tracers. The use of fiber optic A/D serial and signal converters

allows total flexibility in system design and configuration. Since different calibers of tracers have different test requirements, this system can be easily configured to meet different test requirements. It has the ability to discriminate between blind tracers (unlit tracers) and tracers with varying light output. The ability to discern tracers with different light outputs will enable manufacturers to more accurately assess tracer performance and produce more consistent ammunition. More importantly, this methodology removes subjectivity from the measurements and makes them repeatable and consistent.

Future development of this system will focus on expanding to have more channels and perform side-by-side measurements with human observers to begin determining the minimum irradiance required for passing and failing tracers during lot acceptance testing. Additionally, the system will be optimized by evaluating the effect of detector angle and detector distance from the LOF. Further system optimization will enhance the robustness of the overall design and make it easier for manufacturers to implement this system in their testing facilities. ■

ACKNOWLEDGMENTS

The author would like to thank the U.S. Army for funding this program and the International Pyrotechnics Society for permission to republish this article as presented at the International Pyrotechnics Seminar USA. Special thanks to Dr. Anthony Shaw, Michael Pagonis, and Christel Kelly (U.S. Army Combat Capabilities Development Command - Armaments Center) for their helpful comments in preparing this article. Data provided by Dr. Gary Glasperal (U.S. Army Engineer Research and Development Center) is also appreciated.

REFERENCES

- [1] U.S. Army. Technical manual no. 43-0001-27. Washington, DC, 1994.
- [2] DeCusatis, C. *Handbook of Applied Photometry*. Woodbury: American Institute of Physics, 1997.
- [3] Society of Light and Lighting. *SLL Lighting Handbook*. London: CIBSE, 2009.
- [4] Puchalski, W. "The Effect of Angular Velocity and Composition on Pyrotechnic Performance." Defense Technical Information Center (DTIC), Fort Belvoir, VA, <http://www.dtic.mil/dtic/tr/fulltext/u2/a003246.pdf>, 1974.
- [5] Buc, S., G. Adelman, and S. Adelman. "Development of Alternative 7.62 mm Tracer Formulations." DTIC, Fort Belvoir, VA, <http://www.dtic.mil/dtic/tr/fulltext/u2/a335414.pdf>, 1993.
- [6] Briere, P. "The Effect of High Spin on the Performance of Tracer Compositions." *Propellants, Explosives, and Pyrotechnics*, vol. 14, pp. 250–254, 1989.
- [7] U.S. Army Materials Command. *Engineering Design Handbook*, AMCP 706-188, Alexandria, VA, p. 4, 1974.
- [8] Reilly, S. "The Establishment of Threshold Criteria for Automated Acceptance Test Equipment Based on Battlefield Use of Tracer Ammunition." The 26th International Symposium on Ballistics, Miami, FL, pp. 1–8, 2011.
- [9] Conkling, J. *Chemistry of Pyrotechnics*. Boca Raton: CRC Press, 2011.
- [10] Tsai, L., B. Wu, and K. Lin. "Spin Effects on Pyrotechnic Delays of the Molybdenum Family." *Journal of Energetic Materials*, vol. 10, nos. 4–5, pp. 267–285, 1992.
- [11] Dillehay, D. "The Effects of Spin and Liner Thickness on Illuminant Performance." Proceedings of the 11th International Pyrotechnic Seminar, Vail, CO, pp. 103–117, 1986.
- [12] Ontar. PcModWin5 v1.3.1. North Andover, MA, 2010.
- [13] Northrop Grumman. M62 Product Specification. <https://www.northropgrumman.com/Capabilities/7-62mmAmmunition/Documents/M62FactSheet.pdf>, accessed June 2019.
- [14] Boreman, G. D. *Basic Electro-Optics for Electrical Engineers*. SPIE Optical Engineering Press, 1998.

BIOGRAPHY

JAY C. PORET is a physical scientist who has worked in the Pyrotechnics Technology Division of the U.S. Army Combat Capabilities Development Command Armaments Center, Picatinny Arsenal, NJ, since 2003. His research interests include developing optical measurement systems for characterizing military pyrotechnics, developing environmentally benign pyrotechnics, and combustion modeling. Dr. Poret holds a B.S. in ceramic engineering from Rutgers University, an M.S.E. in materials engineering from the University of Alabama at Birmingham, and a Ph.D. in materials science from Johns Hopkins University.

DSIAC JOURNAL: A CALL FOR

ARTICLES

DSIAC is looking for your expertise! Our articles explore new ideas and emerging trends in science and engineering in nine focus areas: Advanced Materials; Autonomous Systems; Directed Energy; Energetics; Military Sensing; Non-Lethal Weapons; Reliability, Maintainability, Quality, Supportability, and Interoperability (RMQSI); Survivability & Vulnerability; and Weapon Systems. If you have an article you would like to submit, please contact Brian Benesch (brian.benesch@dsiac.org).

WINTER 2019 DEADLINES

Abstract: 2 September 2019

Article: 18 October 2019

SPRING 2020 DEADLINES

Abstract: 2 December 2019

Article: 17 January 2020



Discover the **value** of sharing your **DoD-funded research...**

Maximize R&D dollars,
foster collaboration

Advance industry
innovation

Increase peer citations and
worldwide dissemination

Leverage results of
defense-funded research

Ensure long-term availability
and preservation of documents

SUBMIT
your research
today!

R&E Gateway Powered by DTIC
<https://go.usa.gov/xEe7Q>

CONFERENCES AND SYMPOSIA

AUGUST 2019

Space & Missile Defense (SMD) Symposium

6–8 August 2019
Von Braun Center
Huntsville, AL
<https://smdsymposium.org> ▶

2019 Global Explosive Ordnance Disposal (EOD) Symposium & Exhibition

6–8 August 2019
Bethesda North Marriott
Bethesda, MD
<http://www.ndia.org/events/2019/8/6/9950--global-eod> ▶

Fleet Maintenance & Modernization Symposium (FMMS)

7–9 August 2019
San Diego Convention Center
San Diego, CA
<http://www.navalengineers.org/Symposia/FMMS-2019> ▶

2019 Propulsion Energy Forum

19–22 August 2019
JW Marriott
Indianapolis, IN
<https://propulsionenergy.aiaa.org> ▶

Multi-Domain Battle Management Summit

21–23 August 2019
Washington, DC
<https://www.idga.org/events-multidomainbattlemanagement> ▶

Hypersonic Technology & Systems Conference (HTSC)

26–30 August 2019
Springfield, VA
<https://www.usasymposium.com/Hypersonics/2019/default.php> ▶

SEPTEMBER 2019

2019 IEEE/AIAA 38th Digital Avionics Systems Conference (DASC)

8–12 September 2019
<https://2019.dasconline.org> ▶

Conference on Smart Materials, Adaptive Structures, and Intelligent Systems (SMASIS)

9–11 September 2019
Omni Louisville
Louisville, KY
https://event.asme.org/SMASIS?_ga=2.69767120.172949750.1551883560-166280590.1551883560 ▶

Air Vehicle Technology Symposium 2019

10–12 September 2019
Dayton Convention Center
Dayton, OH
<http://www.avtechsymposium.com/index.html> ▶

2019 Air, Space, & Cyber Conference

16–18 September 2019
Gaylord National Resort and Convention Center
National Harbor, MD
<https://www.afa.org/events/calendar/2019-09-16/air-space-cyber-conference> ▶

Modern Day Marine

17–19 September 2019
Brown Field
MCB Quantico, VA
<https://www.marinemilitaryexpos.com/modern-day-marine/home> ▶

2019 IEEE 90th Vehicular Technology Conference (VTC2019-Fall)

22–25 September 2019
Honolulu, HI
https://conferences.ieee.org/conferences_events/conferences/conferencedetails/46249 ▶

Robotics and Autonomous Systems

23–25 September 2019
Detroit, MI
https://roboticsautonomoussystems.iqpc.com/?utm_medium=portal&mac=IQPCCORP ▶

Disruptive Technology for Defence Transformation

24–25 September 2019
Hilton London Canary Wharf
London, UK
https://disruptivetechdefence.iqpc.co.uk/?utm_medium=portal&mac=IQPCCORP ▶

Powder Metallurgy and Additive Manufacturing of Titanium

24–27 September 2019
Salt Lake City, UT
<https://www.mpif.org/Events/PMTi2019Conference.aspx> ▶

Advanced Solid State Lasers Conference

29 September–3 October 2019
Austria Center Vienna
Vienna, Austria
[https://www.osa.org/en-us/meetings/global_calendar/events/advanced_solid_state_lasers_conference_\(1\)](https://www.osa.org/en-us/meetings/global_calendar/events/advanced_solid_state_lasers_conference_(1)) ▶

OCTOBER 2019

2019 IEEE International Integrated Reliability Workshop (IIRW)

13–17 October 2019
South Lake Tahoe, CA
https://conferences.ieee.org/conferences_events/conferences/conferencedetails/47491 ▶

For more events, visit:

dsiac.org/resources/events ▶



Defense Systems
Information Analysis Center

4695 Millennium Drive
Belcamp, MD 21017-1505

DSIAC ONLINE

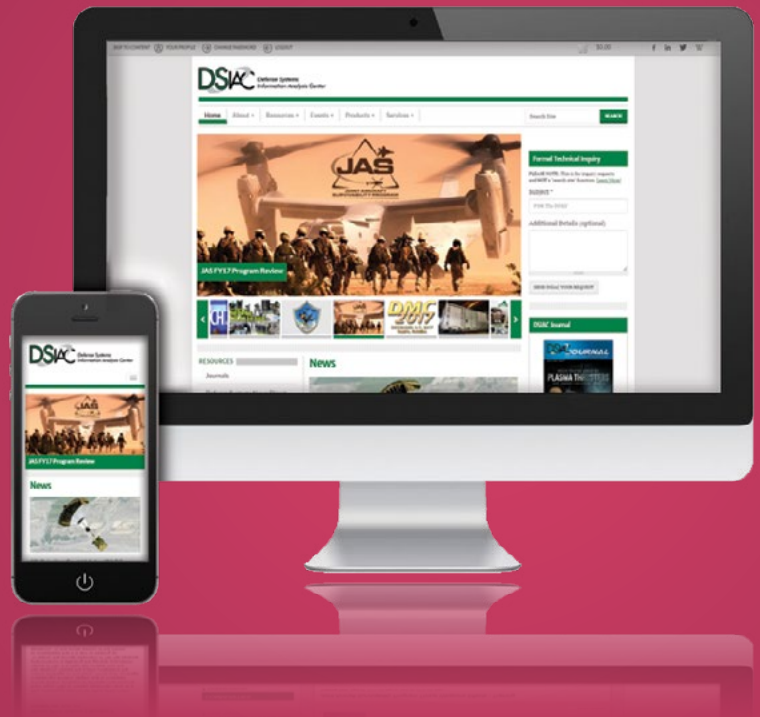
www.dsiac.org

DSIAC PRODUCTS AND SERVICES INCLUDE:

- Performing literature searches.
- Providing requested documents.
- Answering technical questions.
- Providing referrals to subject-matter experts (SMEs).
- Collecting, electronically cataloging, preserving, and disseminating Defense Systems scientific and technical information (STI) to qualified users.
- Developing and deploying products, tools, and training based on the needs of the Defense Systems community.
- Fostering and supporting the DSIAC technical Communities of Practice.
- Participating in key DoD conferences and forums to engage and network with the S&T community.
- Performing customer-funded Core Analysis Tasks (CATs) under pre-competed IDIQ Delivery Orders.

DSIAC SCOPE AREAS INCLUDE:

- Advanced Materials
- Autonomous Systems
- Directed Energy
- Energetics
- Military Sensing
- Non-Lethal Weapons
- Reliability, Maintainability, Quality, Supportability, and Interoperability (RMQSI)
- Survivability and Vulnerability
- Weapon Systems



CONNECT WITH US ON SOCIAL MEDIA!